Heliyon 8 (2022) e11513

Contents lists available at ScienceDirect

Heliyon

journal homepage: www.cell.com/heliyon

Research article

Mathematical model of COVID-19 transmission dynamics incorporating booster vaccine program and environmental contamination

N.I. Akinwande [a], T.T. Ashezua [d], R.I. Gweryina [d,*], S.A. Somma [a], F.A. Oguntolu [a], A. Usman [c], O.N. Abdurrahman [a], F.S. Kaduna [d], T.P. Adajime [e], F.A. Kuta [b], S. Abdulrahman [f], R.O. Olayiwola [a], A.I. Enagi [a], G.A. Bolarin [a], M.D. Shehu [a]

[a] Department of Mathematics, Federal University of Technology Minna, Nigeria
[b] Department of Microbiology, Federal University of Technology, Minna, Nigeria
[c] Department of Statistics, Federal University of Technology, Minna, Nigeria
[d] Department of Mathematics, Federal University of Agriculture, Makurdi, Nigeria
[e] Department of Epidemiology and Community Health, Benue State University, Makurdi, Nigeria
[f] Department of Mathematics, Federal University Birnin Kebbi, Nigeria

ARTICLE INFO

Keywords:
COVID-19
Booster vaccine program
Environmental contamination
Bifurcation
Optimal control analysis

ABSTRACT

COVID-19 is one of the greatest human global health challenges that causes economic meltdown of many nations. In this study, we develop an SIR-type model which captures both human-to-human and environment-to-human-to-environment transmissions that allows the recruitment of corona viruses in the environment in the midst of booster vaccine program. Theoretically, we prove some basic properties of the full model as well as investigate the existence of SARS-CoV-2-free and endemic equilibria. The SARS-CoV-2-free equilibrium for the special case, where the constant inflow of corona virus into the environment by any other means, Ω is suspended ($\Omega = 0$) is globally asymptotically stable when the effective reproduction number $R_{0c} < 1$ and unstable if otherwise. Whereas in the presence of free-living Corona viruses in the environment ($\Omega > 0$), the endemic equilibrium using the centre manifold theory is shown to be stable globally whenever $R_{0c} > 1$. The model is extended into optimal control system and analyzed analytically using Pontryagin's Maximum Principle. Results from the optimal control simulations show that strategy E for implementing the public health advocacy, booster vaccine program, treatment of isolated people and disinfecting or fumigating of surfaces and dead bodies before burial is the most effective control intervention for mitigating the spread of Corona virus. Importantly, based on the available data used, the study also revealed that if at least 70% of the constituents followed the aforementioned public health policies, then herd immunity could be achieved for COVID-19 pandemic in the community.

1. Introduction

The World Health Organization (WHO) reported the outbreak of coronavirus disease (COVID-19) in Wuhan city of China in December 2019. The disease, caused by severe acute respiratory syndrome coronavirus-2 (SARS-CoV-2) [1], spread rapidly over 210 countries across Europe, Asia, sub-Saharan Africa and America, with the utmost prevalence in America. COVID-19 resulted in over 237 million confirmed cases and 4.8 million deaths worldwide [2]. After the first case of COVID-19 on February 27,2020 in Lagos, Nigeria has been one of the leading epicentres of SARS-CoV-2 in Africa, with about 259,007 cases and 3,144 confirmed deaths as at 19th July, 2022 [3]. SARS-CoV-2 is mainly transmitted from one person to another via close contact with infected individuals (dead and alive) [4]. Experimental proofs had it that human corpses are transmissible source of the virus [5], and through human faeces the virus can be shed to the environment [6]. In upholding African traditions and customs of burial practices such as washing of dead bodies before dressing, has in deep sense fuelled the transmission of the virus in Africa [7].

The diagnosis of a probable case was based on the first clinical symptoms such as fever, dry cough, sore throat, loss of smell and taste, head and body aches with, dyspnoea often accompanied by pneumonia [8]

* Corresponding author.
E-mail address: gweryina.reuben@uam.edu.ng (R.I. Gweryina).

https://doi.org/10.1016/j.heliyon.2022.e11513
Received 11 April 2022; Received in revised form 22 July 2022; Accepted 2 November 2022

and exposure to SARS-CoV-2 [9]. The incubation period for SARS-CoV-2 is 2 to 14 days, and most infected persons recover after 2 to 6 weeks of illness [4]. The pandemic nevertheless has recorded a huge rate of mortality, especially among the elderly and people with co-morbidities [10].

Based on the rapid transmissiblity of the virus and fast spreading of the pandemic worldwide, the WHO recommended efforts to curtail the spread of SARS-CoV-2. In the absence of licensed anti-SARS-CoV-2 treatment, these efforts were focused on social distancing, use of face masks, quarantine of suspected cases and isolation of persons infected with SARS-CoV-2 to prevent them from infecting others [8]. At present, COVID-19 vaccine has been developed and administered to individuals globally. However, like any other human vaccines, SARS-CoV-2 vaccine is considered to be imperfect at first dose [11]. Such imperfections can be seen in terms of waning immunity or failure to completely protect the immuned persons against the infection. That is, the primary vaccination series (the first and second doses of COVID-19 vaccine) would allow breakthrough of infection at a reduced rate [12, 13]. Despite all these, it is assumed in this study that the additional dose(s) of booster vaccine will confer permanent immunity to those individuals who received it as reported in [14, 15].

The goal of this study is to examine, through mathematical modelling approach, whether a public health strategy under booster vaccine program and environmental contamination protection can lead to the successful control of SARS-CoV-2. For the purpose of this study, booster vaccine means an extra administration of vaccine dose after primary vaccination series in order to gain complete or lasting immunity. Although many mathematical models have been formulated to assess the impact of anti-SARS-CoV-2 control strategies based on social distancing and face masks, denial effect, quarantine and isolation (see for instance [16, 17, 18, 19, 20, 21]). Few authors [22, 23] investigated the implications of environmental contamination on the transmission dynamics of COVID-19 without considering the shedding from dead bodies. Other researchers formulated mathematical models for assessing the effect of primary vaccination series on the dynamics of COVID-19 without the inclusion of booster vaccine dose(s) [24, 25]. In view of the above, the present study develops a mathematical model for COVID-19 transmission dynamics that enriched the existing works in the following aspects:

i. We incorporate the shedding of SARS-CoV-2 virus from dead bodies as one of the key drivers of COVID-19 transmission based on African perspective.
ii. We include the potential impact of booster vaccine program on the transmission of corona virus.
iii. Apart from shedding of the virus from the infected people and dead bodies into the environment, we add an external source of pool of SARS-CoV-2 (denoted by Ω) to cater for the uncertainty associated with the reservoir of the virus.

The rest of the paper is organized as follows: The new COVID-19 model is formulated in Section 2. Section 3 considers the well-poseness and equilibria analysis of the model. Using partial rank correlation coefficients (PRCCs), sensitivity analysis of model parameters is presented in Section 4 and the optimal control system is analyzed by Pontryagin's maximum principle in Section 5. Simulations of the model to support the theoretical results are presented and discussed in Section 6. The paper is concluded in Section 7.

2. Model formulation

We propose a mathematical model that accounts for the roles of booster vaccine, public health advocacy, environmental contamination and dead bodies on the spread of corona virus. Here, two main epidemiological classes are considered: the human population (alive and dead) and the population of corona virus pathogens present in the environment. Thus, the human population is subdivided into seven classes, namely: susceptible individuals S(t), vaccinated individuals V(t) (who received the first and second doses of the vaccine), Latent individuals L(t), infectious individuals I(t), Isolated/hospitalized individuals Q(t), recovered/protected individuals R(t) and the deceased individuals/dead bodies D(t) at time t, respectively. The population of the corona virus pathogens present in the environment at time t is denoted by P(t). Susceptible individuals are recruited at a constant rate Λ. The susceptible individuals may acquire infection after effective contacts η_1, η_2, η_3 with Latent, infectious individuals and dead bodies respectively. They can also contract the virus via contaminated environment at rate η_4. Both infectious and isolated individuals experience an additional death burden caused by the pandemic at their respective rates δ_1 and δ_2. Dead bodies are buried directly at a rate, ρ. All individuals who are alive may die naturally at a rate μ. Based on the assumption, the environment is contaminated by corona virus at a constant rate Ω, and the respective shedding rates, d_1, d_2, d_3 of the virus from the latent, infectious individuals and the dead bodies. The pathogens decay from the environment at a rate φ via environmental fumigation. Under booster vaccine program, the susceptible humans are given the complete primary vaccine series at a rate ν_1 before attaining lasting immunity via the administration of the booster dose(s) at a rate, ν_2. The vaccine wanes at a rate ω and those vaccinated contracts the virus at reduced rate $(1-\beta)\alpha$, where α is the force of infection defined by equation (1) and β is the degree of protection due to the complete primary series of vaccine administered. Meanwhile, the individuals in the latent class progress to the infectious compartment at a rate σ and gain self-immune recovery at a rate θ, and infectious individuals are isolated at a rate ξ and treated to become permanently protected at a rate γ.

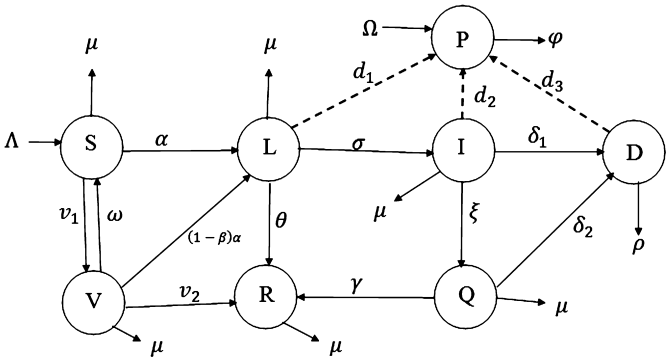

Fig. 1. Flow diagram of COVID-19 transmission dynamics under booster vaccine program and environmental contamination.

$$\alpha = c(1-\epsilon\phi)\left(\frac{\eta_1 L + \eta_2 I + \eta_3 D + \eta_4 P}{N}\right), \tag{1}$$

where

$$N = S + V + L + I + Q + R + D \tag{2}$$

In equation (1), c denotes the number of contacts made between the susceptible and the agents of virus transmission, $\epsilon\phi$ gives the product of public health advocacy and its efficacy. Equation (2) represents the total human population of both the living and the dead. The following assumptions and Fig. 1 were used in deriving equation (3).

A.1 Human dead bodies can still infect susceptible individuals during burials. This assumption is motivated by the African practices such as preparation of dead bodies before dressing. It is supported by the work of [5]
A.2 Both latent and Infectious individuals shed Corona Virus to the environment through human faeces. Dead bodies also shed the virus

Table 1. The parameter values used for numerical simulations.

Parameter	Symbol	Value	Ref.
Recruitment rate of susceptibles	Λ	7,828,143 day^{-1}	estimated
Inflow rate of corona virus into the environment			
by any other means	Ω	148,347,347 day^{-1}	estimated
Degree of protection induced by primary			
vaccination series (first and second doses)	β	0.33	estimated
Shedding rates of the virus from			
(latent, infectious, dead bodies)	(d_1, d_2, d_3)	(0.93,0.067,0.00088) day^{-1}	estimated
COVID-19 induced death rates for			
(infectious, Isolated) individuals	δ_1, δ_2	0.031 day^{-1}	estimated
Effective contact rates for (Latent, infectious)	(η_1, η_2)	$0.82 \in$ (0.1-1.5)	[23]
Effective contact rate of the dead bodies	η_3	0.82	Assumed
Effective contact rate of the pathogens	η_4	$0.82 \in$ (0.1-1.5)	[23]
Rate of administering the primary vaccination series	ν_1	0.71 day^{-1}	estimated
Rate of administering the booster vaccine dose(s)	ν_2	0.29 day^{-1}	estimated
Rate at which the primary vaccine wanes with time	ω	0.02 day^{-1}	Assumed
Isolation rate for infectious individuals	ξ	0.043 day^{-1}	estimated
Self-immune recovery rate for latent individuals	θ	0.072 day^{-1}	estimated
Proper burial rate of dead bodies	ρ	0.95 day^{-1}	Assumed
Decay rate of Corona virus from the environment	φ	0.02 day^{-1}	Assumed
Recovery rate due to treatment	γ	0.94 day^{-1}	estimated
Rate of public health awareness	ϵ	0.9	Assumed
Efficacy rate of public health awareness	ϕ	0.6	Assumed
Number of contacts made	c	0.2 day^{-1}	estimated
Progression rate	σ	0.072 day^{-1}	estimated
Natural death rate	μ	0.01138 day^{-1}	estimated

when the process of burial is improper. This assumption is supported by the work of [6]

A.3 We considered hospitalized individuals to be confined, as such they have negligible contacts with the susceptibles, thus does not contribute in the force of infection.

A.4 We also assumed that poor sanitary practices may result in the promotion of corona virus in the environment. This can be prevalent in the African countries e.g. Nigeria, where poor hygiene is more pronounced.

A.5 We assume that administering booster vaccine dose(s) on vaccinated people and recovery after infection yields lasting immunity/protection for a particular variant of the disease. This is supported by the reports given in [14, 15, 26].

A.6 We considered the recruitment of corona virus pathogens into the environment at a constant rate due to uncertainty since the source of the virus is not yet confirmed at the moment. This assumption is supported by the works of [27, 28].

The parameter values for the model are summarized in Table 1.

$$\begin{aligned}
\frac{dS(t)}{dt} &= \Lambda + \omega V - \alpha S - (\mu + \nu_1)S,\\
\frac{dV(t)}{dt} &= \nu_1 S - (\mu + \omega + \nu_2 + (1-\beta)\alpha)V,\\
\frac{dL(t)}{dt} &= \alpha S + (1-\beta)\alpha V - (\mu + \sigma + \theta)L,\\
\frac{dI(t)}{dt} &= \sigma L - (\mu + \xi + \delta_1)I,\\
\frac{dQ(t)}{dt} &= \xi I - (\mu + \gamma + \delta_2)Q.\\
\frac{dR(t)}{dt} &= \nu_2 V + \theta L + \gamma Q - \mu R,\\
\frac{dD(t)}{dt} &= \delta_1 I + \delta_2 Q - \rho D,\\
\frac{dP(t)}{dt} &= \Omega + d_1 L + d_2 I + d_3 D - \varphi P,
\end{aligned} \tag{3}$$

System (3) is obviously accompanied with the initial conditions $S(0) = S_0, V(0) = V_0, L(0) = L_0, I(0) = I_0, Q(0) = Q_0, R(0) = R_0, D(0) = D_0, P(0) = P_0$.

Adding the first six equations of the system above gives the conservation equation

$$\frac{dG(t)}{dt} = \Lambda - \mu G - \delta_1 I - \delta_2 Q, \tag{4}$$

where $G = S + V + L + I + Q + R$ is the total human population that are alive.

3. Boundedness, invariance and equilibria analysis

3.1. Boundedness and invariance

Lemma 3.1. *Suppose the system (3) has a global solution with respect to the non-negative initial conditions. Then the solution is non-negative at all time.*

Proof. Assume that $S(0) \geq 0, V(0) \geq 0, L(0) \geq 0, I(0) \geq 0, Q(0) \geq 0, R(0) \geq 0, D(0) \geq 0$ and $P(0) \geq 0$. The first equation of System (3) can take the form

$$\frac{dS(t)}{dt} \geq \Lambda - B(t)S,$$

where $B(t) = \mu + \alpha$. This linear first order equation has a solution

$$S(t) = S(0)exp\Big(\int_0^t -B(s)ds\Big) + exp\Big(\int_0^t -B(s)ds\Big) \times \int_0^t \Lambda exp\Big(\int_0^w B(u)du\Big)dw \geq 0.$$

From the second equation of system (3), we have

$$\frac{dV(t)}{dt} = \nu_1 S - (\mu + \omega + \nu_2 + (1-\beta)\alpha)V \geq -(\mu + \omega + \nu_2 + (1-\beta)\alpha)V,$$

This implies that

$$V(t) = V(0)exp\Big[-(\mu+\omega+\nu_2)t\Big] \times exp\Big[-(1-\beta)\int_0^t \alpha(s)ds\Big] > 0$$

Thus, $S(0) \geq 0, V(0) \geq 0 \forall t \geq 0$. In a like manner, it can be shown known that $L(0) \geq 0, I(0) \geq 0, Q(0) \geq 0, R(0) \geq 0, D(0) \geq 0$ and $P(0) \geq 0$ for all $t > 0$. This completes the proof. □

The proof of boundedness of system (3) is provided in Lemma 3.2.

Lemma 3.2. *Suppose the given initial conditions of system (3) satisfy* $G(0) \leq G_n$, $D(0) \leq D_n$, $P(0) \leq P_n$, *where* $G_n = \frac{\Lambda}{\mu}$, $D_n = \frac{(\delta_1+\delta_2)\Lambda}{\mu\rho}$ *and* $P_n = \frac{\Omega}{\varphi} + \frac{(d_1+d_2+d_3)\Lambda}{\mu\varphi}$. *Then the solution when exist on interval I, satisfies the following bounds:* $G(t) \leq G_n$, $D(t) \leq D_n$, $P(t) \leq P_n$.

Proof. In the absence of COVID-19 related deaths $\delta_1 = \delta_2 = 0$, we obtain from equation (4) that

$$\frac{dG(t)}{dt} \leq \Lambda - \mu G.$$

Onward integration gives

$$G(t) \leq \frac{\Lambda}{\mu} + (G(0) - \frac{\Lambda}{\mu})exp(-\mu t).$$

Thus, $G(t) \leq G_n$ whenever $G(0) \leq G_n$. Since $I(t) \leq G_n$ and $Q(t) \leq G_n$, we see that the seventh equation of the system (3) yields

$$\frac{dD(t)}{dt} \leq (\delta_1+\delta_2)G_n - \rho D$$

from which we obtain $D(t) \leq D_n$. In addition, the last equation of system (3) can be given as

$$\frac{P(t)}{dt} \leq \Omega + (d_1+d_2+d_3)G_n - \varphi P$$

and consequently accounts for $P(t) \leq P_n$. From the above Lemmas 3.1 and 3.2, we have the following theorem

Theorem 3.3. *The closed set* $C_\Omega^{\mathbb{R}} = \Big\{(S(t), V(t), L(t), I(t), Q(t), R(t), D(t), P(t)) \in \mathbb{R}_+^8 : G(t) \leq \frac{\Lambda}{\mu}, D(t) \leq \frac{(\delta_1+\delta_2)\Lambda}{\mu\rho}, P(t) \leq \frac{\Omega}{\varphi} + \frac{(d_1+d_2+d_3)\Lambda}{\mu\varphi}\Big\}$. *is positively invariant and attracting for all non-negative starting conditions in* $\mathbb{R}_+^8$.

However, for the special case ($\Omega = 0$), the dynamical behaviour of the system may be found biologically useful within the feasible region $C_0^{\mathbb{R}}$.

Theorem 3.4. *The closed set* $C_0^{\mathbb{R}} = \Big\{(S(t), V(t), L(t), I(t), Q(t), R(t), D(t), P(t)) \in \mathbb{R}_+^8 : G(t) \leq \frac{\Lambda}{\mu}, D(t) \leq \frac{(\delta_1+\delta_2)\Lambda}{\mu\rho}, P(t) \leq \frac{(d_1+d_2+d_3)\Lambda}{\mu\varphi}\Big\}$. *for the system (3) at* $\Omega = 0$ *is positively invariant and attracting for all non-negative initial conditions in* $\mathbb{R}_+^8$. □

3.2. Equilibria analysis

3.2.1. Stability of SARS-CoV-2-free equilibrium

In this subsection, we consider the situation where there is no presence of corona virus in the environment ($\Omega = 0$). This scenario refers to SARS-CoV-2 free equilibrium, E_0. However, when $\Omega > 0$, no disease-free equilibrium exists. Following system (3), we have $E_0(S^0, V^0, L^0, I^0, Q^0, R^0, D^0, P^0)$, where

$$S^0 = \frac{\Lambda(\mu+\omega+\nu_2)}{\mu(\mu+\omega+\nu_2)+\nu_1(\mu+\nu_2)}, \quad V^0 = \frac{\nu_1\Lambda}{\mu(\mu+\omega+\nu_2)+\nu_1(\mu+\nu_2)},$$
$$L^0 = 0, \quad I^0 = 0, \quad D^0 = 0, \quad Q^0 = 0, \quad P^0 = 0,$$
$$R^0 = \frac{\Lambda\nu_1\nu_2}{\mu\Big[\mu(\mu+\omega+\nu_2)+\nu_1(\mu+\nu_2)\Big]},$$

The system (3) at $\Omega = 0$ can be rewritten as in equation (5)

$$\dot{x} = f(x) = H(x) - U(x), \tag{5}$$

where

$$H(x) = \begin{pmatrix} \alpha(S+(1-\beta)V) \\ 0 \\ 0 \\ 0 \\ 0 \end{pmatrix} \quad \text{and} \quad U(x) = \begin{pmatrix} (\mu+\sigma+\theta)L \\ -\sigma L + (\mu+\xi+\delta_1)I \\ -\xi I + (\mu+\gamma+\delta_2)Q \\ -\delta_1 I - \delta_2 Q + \rho D \\ -d_1 L - d_2 I - d_3 D + \varphi P \end{pmatrix},$$

are the new infections and transfer terms respectively. Evaluating the Jacobian of $H(x)$ and $U(x)$ at SARS-CoV-2-free equilibrium E_0 gives

$$F = \begin{pmatrix} \kappa\eta_1 & \kappa\eta_2 & 0 & \kappa\eta_3 & \kappa\eta_4 \\ 0 & 0 & 0 & 0 & 0 \\ 0 & 0 & 0 & 0 & 0 \\ 0 & 0 & 0 & 0 & 0 \\ 0 & 0 & 0 & 0 & 0 \end{pmatrix} \quad \text{and}$$

$$V = \begin{pmatrix} \mu+\sigma+\theta & 0 & 0 & 0 & 0 \\ -\sigma & \mu+\xi+\delta_1 & 0 & 0 & 0 \\ 0 & -\xi & \mu+\gamma+\delta_2 & 0 & 0 \\ 0 & -\delta_1 & -\delta_2 & \rho & 0 \\ -d_1 & -d_2 & 0 & -d_3 & \varphi \end{pmatrix},$$

with the inverse of V given by

$$V^{-1} = \begin{pmatrix} \frac{1}{q_m} & 0 & 0 & 0 & 0 \\ \frac{\sigma}{q_m q_w} & \frac{1}{q_w} & 0 & 0 & 0 \\ \frac{\xi\sigma}{q_m q_w q_n} & \frac{\xi}{q_w q_n} & \frac{1}{q_n} & 0 & 0 \\ \sigma\frac{\xi\delta_2+\delta_1 q_n}{\rho q_m q_w q_n} & \frac{\xi\delta_2+\delta_1 q_n}{\rho q_w q_n} & \frac{\delta_2}{\rho q_n} & \frac{1}{\rho} & 0 \\ \frac{\rho q_n(d_2\sigma+q_w d_1)+d_3\sigma(\xi\delta_2+q_n\delta_1)}{\rho\varphi q_m q_w q_n} & \frac{\rho q_n d_2+d_3(\xi\delta_2+q_n\delta_1)}{\rho\varphi q_w q_n} & \frac{d_3\delta_2}{\rho\varphi q_n} & \frac{d_3}{\rho\varphi} & \frac{1}{\varphi} \end{pmatrix},$$

where $q_m = \mu+\sigma+\theta, q_w = \mu+\xi+\delta_1$ and $q_n = \mu+\gamma+\delta_2$.

The largest eigenvalue of the next generation matrix FV^{-1} denoted by R_{0c} is given by

$$R_{0c} = \frac{\kappa\eta_1}{q_m} + \frac{\kappa\eta_2\sigma}{q_m q_w} + \kappa\eta_3\sigma\frac{\xi\delta_2+\delta_1 q_n}{\rho q_m q_w q_n} + \kappa\eta_4\frac{\rho q_n(d_2\sigma+q_w d_1)+d_3\sigma(\xi\delta_2+q_n\delta_1)}{\rho\varphi q_m q_w q_n}. \tag{6}$$

with

$$\kappa = c(1-\epsilon\phi)\frac{\mu H_0}{\mu(\mu+\omega+\nu_2)+\nu_1(\mu+\nu_2)}.$$

and $H_0 = \mu+\omega+\nu_2+(1-\beta)\nu_1$. The effective reproduction number R_{0c} is defined as the expected number of secondary COVID-19 cases produced by one infected individual during its entire period of infectiousness in an entire susceptible population in the presence of control strategies [29]. We observe from equation (6) that R_{0c} is given as the sum of four infection contributions:

(i) $R_{0c}^L = \frac{\kappa\eta_1}{q_m}$, is the contribution of Latent humans, L;
(ii) $R_{0c}^I = \frac{\kappa\eta_2\sigma}{q_m q_w}$, is the contribution of infectious humans, I;
(iii) $R_{0c}^D = \kappa\eta_3\sigma\frac{\xi\delta_2+\delta_1 q_n}{\rho q_m q_w q_n}$, is the contribution due to the handling of dead bodies. That is, infected corpses, D;
(iv) $R_{0c}^P = \kappa\eta_4\frac{\rho q_n(d_2\sigma+q_w d_1)+d_3\sigma(\xi\delta_2+q_n\delta_1)}{\rho\varphi q_m q_w q_n}$, is the contribution due to the environmental contamination by the SARS-CoV-2 virus, P.

From the well-known Theorem 2 of [29], the following result holds

Theorem 3.5. *The SARS-free equilibrium, E_0 of the system (3) in $C_0^{\mathbb{R}}$ is locally asymptotically stable if $R_{0c} \leq 1$ and unstable if $R_{0c} > 1$.*

Proof. The stability of E_0 is established from the roots of the characteristic polynomial, which says that the equilibrium is stable if the roots of the characteristic polynomial are all real and negative. Now, at E_0, the Jacobian matrix of system (3) is defined by

$$J(E_0) = \begin{pmatrix} -q_x & \omega & -n_p & -n_r & 0 & 0 & -m_p & -m_r \\ \nu_1 & -q_y & -n_q & -n_w & 0 & 0 & -m_q & -m_w \\ 0 & 0 & q_z & m_x & 0 & 0 & m_y & m_z \\ 0 & 0 & \sigma & -q_w & 0 & 0 & 0 & 0 \\ 0 & 0 & 0 & \xi & -q_n & 0 & 0 & 0 \\ 0 & \nu_2 & \theta & 0 & \gamma & -\mu & 0 & 0 \\ 0 & 0 & 0 & \delta_1 & \delta_2 & 0 & -\rho & 0 \\ 0 & 0 & d_1 & d_2 & 0 & 0 & d_3 & -\varphi \end{pmatrix},$$

with $q_x = \mu + \nu_1$, $q_y = \mu + \omega + \nu_2$, $q_w = \mu + \xi + \delta_1$, $q_n = \mu + \gamma + \delta_2$, $n_p = c(1-\epsilon\phi)\eta_1 \frac{S^0}{N}$, $n_q = c(1-\epsilon\phi)(1-\beta)\eta_1 \frac{V^0}{N}$, $q_z = n_p + n_q - (\mu+\sigma+\theta)$, $n_r = c(1-\epsilon\phi)\eta_2 \frac{S^0}{N}$, $n_w = c(1-\epsilon\phi)(1-\beta)\eta_2 \frac{V^0}{N}$, $m_p = c(1-\epsilon\phi)\eta_3 \frac{S^0}{N}$, $m_q = c(1-\epsilon\phi)(1-\beta)\eta_3 \frac{V^0}{N}$, $m_r = c(1-\epsilon\phi)\eta_4 \frac{S^0}{N}$, $m_w = c(1-\epsilon\phi)(1-\beta)\eta_4 \frac{V^0}{N}$, $m_y = m_p + m_q$ and $m_z = m_r + m_w$. The characteristic polynomial is given by

$$(-\mu - \lambda_e)(\lambda_e^7 + A_6\lambda_e^6 + A_5\lambda_e^5 + A_4\lambda_e^4 + A_3\lambda_e^3 + A_2\lambda_e^2 + A_1\lambda_e + A_0) = 0, \quad (7)$$

where,

$$\begin{aligned}
A_6 &= \rho + \varphi + q_x + q_y - q_m(R_{0c}^L - 1) + q_w + q_n, \\
A_5 &= (q_x q_y - \omega\nu_1) + (q_x + q_y)(q_w + q_n) + \rho(\varphi + q_x + q_y + q_w + q_n) \\
&\quad + \varphi(q_x + q_y + q_w + q_n) + q_w q_n\Big[1 - \frac{\kappa\eta_2\sigma}{q_w q_n} - \frac{d_1\kappa\eta_4\sigma}{q_w q_n}\Big] \\
&\quad - q_m(R_{0c}^L - 1)(\rho + \varphi + q_x + q_y + q_w + q_n), \\
A_4 &= -\kappa\eta_2\sigma(\rho + \varphi + q_x + q_y + q_n) - q_m(R_{0c}^L - 1)\Big[\rho(\varphi + q_x + q_y + q_w + q_n) \\
&\quad + \varphi(q_x + q_y + q_w + q_n) + q_x q_y - \omega\nu_1 + (q_x + q_y)(q_w + q_n) + q_w q_n\Big] \\
&\quad - \kappa\eta_4\Big[d_1(\rho + q_x + q_y + q_w + q_n) + d_2\sigma\Big] - \kappa\eta_3\delta_1 \\
&\quad + \rho\Big[(q_x + q_y)(q_w + q_n) + q_w q_n + q_x q_y - \omega\nu_1] + \rho\varphi(q_x + q_y + q_w + q_n) \\
&\quad + \varphi\Big[(q_x + q_y)(q_w + q_n) + q_w q_n + q_x q_y - \omega\nu_1\Big] + q_w(q_x q_y - \omega\nu_1 + q_x q_n) \\
&\quad + q_n(q_y q_w + q_x q_y - \omega\nu_1), \\
A_3 &= -q_m q_w\Big[(R_{0c}^L - 1 + \rho R_{oc}^I)\Big(\rho\varphi + q_n(\rho + \varphi) + (q_x + q_y)(\rho + \varphi + q_n) \\
&\quad + q_x q_y - \omega\nu_1\Big) + \rho q_n R_{0c}^D\Big] - \kappa\eta_3\sigma\delta_1(\varphi + q_x + q_y) \\
&\quad - q_m q_n(R_{0c}^L - 1)\Big[\rho\varphi + (\rho + \varphi)(q_x + q_y) + q_x q_y - \omega\nu_1\Big] \\
&\quad - q_m q_n(R_{0c}^L - 1)\Big[(\rho + \varphi)(q_x q_y - \omega\nu_1) + \rho\varphi(q_x + q_y)\Big] \\
&\quad + q_n\Big[(\varphi + q_w)(q_x q_y - \omega\nu_1) + \rho\varphi q_w + (q_x + q_y)(\rho\varphi + q_w(\rho + \varphi))\Big] \\
&\quad + \rho\varphi\Big[q_x q_y - \omega\nu_1 + q_w(q_x + q_y)\Big] + (q_x q_y - \omega\nu_1)\Big[\varphi q_w + \rho(q_w + q_n)\Big] \\
&\quad - \kappa\eta_4\sigma\Big[d_2(\rho + q_y + q_n) + \delta_1(d_3 + q_n)] - \kappa\eta_4 d_1\Big[\rho(q_x + q_y + q_w + q_n) \\
&\quad + q_w(q_x + q_y + q_n) + q_n(q_x + q_y) + q_x q_y - \omega\nu_1\Big], \\
A_2 &= \rho\varphi q_m q_w q_n(1 - R_{0c}) + q_m q_w(1 - R_{0c}^L - R_{0c}^I)\Big[(q_x + q_y)(\rho\varphi + q_n(\rho + \varphi)) \\
&\quad + (q_x q_y - \omega\nu_1)(\rho + \varphi)\Big] \\
&\quad + q_m q_w q_n(q_x q_y - \omega\nu_1)\Big[1 - R_{0c}^L - R_{0c}^I - \rho R_{0c}^D\Big(\frac{q_x + q_y}{q_x + q_y - \omega\nu_1}\Big)\Big] \\
&\quad + (q_x q_y - \omega\nu_1)\Big[\rho\varphi(q_w + q_n) + q_w q_n(\rho + \varphi + \rho\varphi(q_x + q_y))\Big] \\
&\quad + q_m(1 - R_{0c}^L)\Big[\rho\varphi q_n(q_x + q_y) + (q_x q_y - \omega\nu_1)(\rho\varphi + q_n(\rho + \varphi))\Big] \\
&\quad - \kappa\eta_4\Big[(\rho d_1 + d_2\omega)(q_x q_y - \omega\nu_1) + d_2\sigma q_n q_y\Big] \\
&\quad - \kappa\eta_4 d_1(q_w + q_n)\Big[q_x q_y - \omega\nu_1 + \rho q_x + d_1 q_y\Big] \\
&\quad - \kappa\eta_3\sigma\Big[\delta_1(q_x q_y - \omega\nu_1) + \varphi(\xi\delta_2 + q_x\delta_1)\Big] \\
&\quad - \kappa\eta_3(q_x + q_y)\Big[d_1 q_w q_n + \sigma(\rho d_2 + d_3\delta_1)\Big] \\
&\quad - \kappa\eta_4(q_x + q_y)\Big[d_1 q_w q_n + \sigma(\xi\delta_2 + \delta_1 q_n + \rho d_2 + d_3\delta_1)\Big], \\
A_1 &= -q_m q_w q_n\Big[(R_{0c}^L - 1)(\rho\varphi(q_x + q_y) + (\rho + \varphi)(q_x q_y - \omega\nu_1)) \\
&\quad + R_{0c}^I(\rho + \varphi)(q_x q_y - \omega\nu_1) + R_{0c}^P\rho\varphi(q_x + q_y) + \rho R_{0c}^D(\varphi(q_x + q_y) \\
&\quad + q_x q_y - \omega\nu_1)\Big] - \kappa\eta_3\sigma\varphi\delta_1(q_x q_y - \omega\nu_1) \\
&\quad - \kappa\eta_4(d_3\sigma\delta_1 + q_n(q_x q_y - \omega\nu_1)(d_2\sigma + \rho d_1 + q_w d_1)) \\
&\quad + \rho\varphi q_w q_n(q_x q_y - \omega\nu_1)\Big[1 - \frac{\kappa\eta_2\sigma}{q_w q_n}\Big(1 + q_n\frac{q_x + q_y}{q_x q_y - \omega\nu_1}\Big) \\
&\quad - q_m(R_{0c}^L - 1)\Big(\frac{q_w + q_n}{q_w q_n}\Big)\Big], \\
A_0 &= \rho\varphi q_m q_w q_n H_0(1 - R_{0c}).
\end{aligned}$$

According to [30], if $A_6, A_5, A_4, A_3, A_2, A_1, A_0$ are positive, then the roots of equation (7) have negative real parts whenever $R_{0c} < 1$. Thus, the SARS-CoV-2-free equilibrium, E_0 is locally asymptotically stable since $A_i > 0, i = 0, 1, 2, ..., 6$ when $R_{0c} < 1$. However when the $R_{0c} > 1, A_0 < 0$. This implies that positive real parts exist, as such E_0 is unstable if $R_{0c} > 1$. □

For the global stability, we prove the following result

Theorem 3.6. *The SARS-CoV-2-free equilibrium, E_0 of the system (3) in $C_0^{\mathbb{R}}$ is globally asymptotically stable if $R_{0c} \leq 1$ and unstable otherwise*

Proof. As in [31], we consider a Lyapunov function $\Phi_f = L$. From the system (3) at $\Omega = 0$ by setting $\frac{dI}{dt} = \frac{dQ}{dt} = \frac{dD}{dt} = \frac{dP}{dt} = 0$, we obtain

$$\begin{cases} I = \dfrac{\sigma L}{\mu + \xi + \delta_1}, \\ Q = \dfrac{\xi\sigma L}{(\mu + \xi + \delta_1)(\mu + \gamma + \delta_2)}, \\ D = \Big[\dfrac{\delta_1\sigma}{\rho(\mu + \xi + \delta_1)} + \dfrac{\delta_2\xi\sigma}{\rho(\mu + \xi + \delta_1)(\mu + \gamma + \delta_2)}\Big]L, \\ P = \Big[\dfrac{d_1}{\varphi} + \dfrac{d_2\sigma}{\varphi(\mu + \xi + \delta_1)} + \dfrac{d_5\sigma(\delta_2\xi + \delta_1(\mu + \gamma + \delta_2))}{\rho\varphi(\mu + \xi + \delta_1)(\mu + \gamma + \delta_2)}\Big]L. \end{cases} \quad (8)$$

Thus,

$$\begin{aligned}
\frac{d\Phi_f}{dt} &= \frac{dL}{dt} \\
&= c(1 - \epsilon\phi)(\eta_1 L + \eta_2 I + \eta_3 D + \eta_4 P)\Big(\frac{S}{N} + (1 - \beta)\frac{V}{N}\Big) - (\mu + \sigma + \theta)L.
\end{aligned}$$

Plugging in the equation (8) into the above gives

$$\begin{aligned}
\frac{d\Phi_f}{dt} &= c(1 - \epsilon\phi)\Big(\frac{S}{N} + (1 - \beta)\frac{V}{N}\Big)\Big[\eta_1 + \frac{\eta_2\sigma}{\mu + \xi + \delta_1} \\
&\quad + \eta_3\Big(\frac{\delta_1\sigma}{\rho(\mu + \xi + \delta_1)} + \frac{\delta_2\xi\sigma}{\rho(\mu + \xi + \delta_1)(\mu + \gamma + \delta_2)}\Big) \\
&\quad + \eta_4\Big(\frac{d_1}{\varphi} + \frac{d_2\sigma}{\varphi(\mu + \xi + \delta_1)} \\
&\quad + \frac{d_5\sigma(\delta_2\xi + \delta_1(\mu + \gamma + \delta_2))}{\rho\varphi(\mu + \xi + \delta_1)(\mu + \gamma + \delta_2)}\Big)\Big]L - (\mu + \sigma + \theta)L.
\end{aligned}$$

Recall that at SARS-CoV-2-free equilibrium

$$\frac{S}{N} \leq \frac{S^0}{N^0} \quad \text{and} \quad \frac{V}{N} \leq \frac{V^0}{N^0}.$$

Therefore,

$$\begin{aligned}\frac{d\Phi_f}{dt} &\le c(1-\epsilon\phi)\Big(\frac{S^0}{N^0}+(1-\beta)\frac{V^0}{N^0}\Big)\Big[\eta_1+\frac{\eta_2\sigma}{\mu+\xi+\delta_1}\\ &+\eta_3\Big(\frac{\delta_1\sigma}{\rho(\mu+\xi+\delta_1)}+\frac{\delta_2\xi\sigma}{\rho(\mu+\xi+\delta_1)(\mu+\gamma+\delta_2)}\Big)\\ &+\eta_4\Big(\frac{d_1}{\varphi}+\frac{d_2\sigma}{\varphi(\mu+\xi+\delta_1)}\\ &+\frac{d_5\sigma(\delta_2\xi+\delta_1(\mu+\gamma+\delta_2))}{\rho\varphi(\mu+\xi+\delta_1)(\mu+\gamma+\delta_2)}\Big)\Big]L-(\mu+\sigma+\theta)L,\\ &\le(\mu+\sigma+\theta)\Big(R_{0c}-1\Big)L.\end{aligned}$$

Clearly, $\frac{d\Phi_f}{dt}\le 0$ (negative semi definite) when $R_{0c}\le 1$ and equality holding when $R_{0c}=1$. Thus, the largest compact set C_0^R such that $\frac{d\Phi_f}{dt}=0$ when $R_{0c}\le 1$ is the singleton E_0. Hence, by LaSalle invariance principle [32], the SARS-CoV-2 free equilibrium is globally asymptotically stable in $C_0^{\mathbb{R}}$ and unstable otherwise. □

3.2.2. Stability of SARS-CoV-2-endemic equilibrium

Here, we investigated the existence of equilibrium points of equations (3) and noted from the model that, the presence of the constant recruitment rate Ω (if always positive) of the virus into the environment makes the disease-free equilibrium of the system unobtainable. This sounds unique as far as COVID-19 model is concerned. Our justification for this assumption is that, the main reservoir for SARS-CoV-2 is still under scientific investigations [27, 28]. Let $E^{**}=\Big(S^{**},V^{**},L^{**},I^{**},Q^{**},R^{**},D^{**},P^{**}\Big)$ be an equilibrium solution of the following equation:

$$\begin{aligned}0&=\Lambda+\omega V^{**}-\alpha^{**}S^{**}-(\mu+\nu_1)S^{**},\\ 0&=\nu_1S^{**}-(\mu+\omega+\nu_2+(1-\beta)\alpha^{**})V^{**},\\ 0&=\alpha^{**}S^{**}+(1-\beta)\alpha^{**}V^{**}-(\mu+\sigma+\theta)L^{**},\\ 0&=\sigma L^{**}-(\mu+\xi+\delta_1)I^{**},\\ 0&=\xi I^{**}-(\mu+\gamma+\delta_2)Q^{**}.\\ 0&=\nu_2V^{**}+\theta L^{**}+\gamma Q^{**}-\mu R^{**},\\ 0&=\delta_1I^{**}+\delta_2Q^{**}-\rho D^{**},\\ 0&=\Omega+d_1L^{**}+d_2I^{**}+d_3D^{**}-\varphi P^{**}.\end{aligned}\tag{9}$$

Then, we obtained the expressions in (10) from system (9) after a lengthy algebraic calculation.

$$\begin{aligned}S^{**}&=\frac{\Lambda(\mu+\omega+\nu_2+(1-\beta)\alpha^{**})}{f(\alpha^{**})},\quad V^{**}=\frac{\nu_1\Lambda}{f(\alpha^{**})},\\ L^{**}&=\frac{\alpha^{**}\Lambda\Big[(1-\beta)\alpha^{**}+H_0\Big]}{(\mu+\sigma+\theta)f(\alpha^{**})},\\ I^{**}&=Y_1\frac{\alpha^{**}\Lambda\Big[(1-\beta)\alpha^{**}+H_0\Big]}{(\mu+\sigma+\theta)f(\alpha^{**})},\quad Q^{**}=Y_2\frac{\alpha^{**}\Lambda\Big[(1-\beta)\alpha^{**}+H_0\Big]}{(\mu+\sigma+\theta)f(\alpha^{**})},\\ D^{**}&=Y_3\frac{\alpha^{**}\Lambda\Big[(1-\beta)\alpha^{**}+H_0\Big]}{(\mu+\sigma+\theta)f(\alpha^{**})},\quad P^{**}=\frac{\Omega}{\varphi}+\frac{Y_4}{\varphi}\frac{\alpha^{**}\Lambda\Big[(1-\beta)\alpha^{**}+H_0\Big]}{(\mu+\sigma+\theta)f(\alpha^{**})},\\ R^{**}&=\frac{\Lambda g(\alpha^{**})}{\mu(\mu+\sigma+\theta)f(\alpha^{**})},\end{aligned}\tag{10}$$

where

$$\begin{aligned}Y_1&=\frac{\sigma}{\mu+\xi+\delta_1},\quad Y_2=\frac{\xi Y_1}{\mu+\gamma+\delta_2},\quad Y_3=\frac{\delta_1Y_1+\delta_2Y_2}{\rho},\\ Y_4&=d_1+d_2Y_1+d_3Y_3,\\ f(\alpha^{**})&=(1-\beta)(\alpha^{**})^2+\Big[\mu+\omega+\nu_2+(1-\beta)(\mu+\nu_1)\Big]\alpha^{**}\\ &\quad+\mu(\mu+\omega+\nu_2)+\nu_1(\mu+\nu_2),\\ g(\alpha^{**})&=(1-\beta)(\theta+\gamma Y_2)(\alpha^{**})^2+H_0(\theta+\gamma Y_2)\alpha^{**}+\nu_1\nu_2(\mu+\sigma+\theta),\end{aligned}$$

and α^{**} is the solution of the cubic equation (11)

$$B_3(\alpha^{**})^3+B_2(\alpha^{**})^2+B_1\alpha^{**}-B_0=0,\tag{11}$$

where

$$\begin{aligned}B_3&=\varphi\Lambda(1-\beta)\Big[\theta+\gamma Y_2+\mu(1+\sum_{i=1}^{3}Y_i)\Big],\\ B_2(\Omega)&=\Lambda\mu\varphi(1-\beta)(\mu+\sigma+\theta)\Big[1-R_{0c}\Big(\frac{\mu(\mu+\omega+\nu_2)+\nu_1(\mu+nu_2)}{\mu H_0}\Big)\Big]\\ &\quad+\Lambda\varphi H_0\Big[\theta+\gamma Y_2+\mu(1+\sum_{i=1}^{3}Y_i)\Big]-\Omega\mu\eta_4c(1-\epsilon\phi)(1-\beta)(\mu+\sigma+\theta)\\ B_1(\Omega)&=\Lambda\varphi(\mu+\sigma+\theta)\Big[\mu(\mu+\omega+\nu_2)+\nu_1(\mu+\nu_2)\Big](1-R_{0c})\\ &\quad-\Omega\mu c(1-\epsilon\phi)\eta_4(\mu+\sigma+\theta)\Big[\mu+\omega+\nu_2+(1-\beta)(\mu+\nu_1)\Big],\\ B_0(\Omega)&=\Omega\eta_4c(1-\epsilon\phi)\mu(\mu+\sigma+\theta)\Big[\mu(\mu+\omega+\nu_2)+\nu_1(\mu+\nu_2)\Big]\end{aligned}$$

It is obvious that $B_0(0)=0$ if $\Omega=0$, then $\alpha^{**}=0$ is a root of this cubic equation (11), that defines the SARS-CoV-2 free equilibrium and a unique positive root of equation (11) exists if and only if $B_1(0)<0$ which is possible with $R_{0c}>1$. Consequently, equation (11) reduces to the following

$$F(\alpha^{**})=B_3(\alpha^{**})^2+B_2(0)\alpha^{**}+B_1(0)=0,\tag{12}$$

where B_3 remains the same as above, but

$$\begin{aligned}B_2(0)&=\Lambda\mu\varphi(1-\beta)(\mu+\sigma+\theta)\Big[1-R_{0c}\Big(\frac{\mu(\mu+\omega+\nu_2)+\nu_1(\mu+nu_2)}{\mu H_0}\Big)\Big]\\ &\quad+\Lambda\varphi H_0\Big[\theta+\gamma Y_2+\mu(1+\sum_{i=1}^{3}Y_i)\Big]\\ B_1(0)&=\Lambda\varphi(\mu+\sigma+\theta)\Big[\mu(\mu+\omega+\nu_2)+\nu_1(\mu+\nu_2)\Big](1-R_{0c}).\end{aligned}\tag{13}$$

The endemic equilibria of the system (13) at $\Omega=0$ with α^{**} a positive root of equation (12). Note that negative endemic equilibria are biologically meaningless, the conditions for $F(\alpha^{**})$ to have positive real zeros are determined below.

Suppose $0\le\beta<1$. Then clearly, $B_3>0$ and so the quadratic $F(\alpha^{**})$ concave upwards. We carry out a case analysis just as in [33] to obtain the number of positive real zeros of F.

Case 1. Suppose that $R_{0c}>1$. Then $B_1(0)<0$ and so the vertical intercept of $F(\alpha^{**})$ is negative. Adding to the fact that F is quadratic, it follows that it has two real roots of opposite signs. Therefore, the system (3) has a unique positive equilibrium when $R_{0c}>1$.

Case 2. Suppose that $R_{0c}=1$. Then $B_1(0)<0$. Thus, the quadratic reduces to $F(\alpha^{**})=B_3(\alpha^{**})^2+B_2(0)\alpha^{**}$, with $\alpha^{**}=0$ (for disease-free equilibrium) and $\alpha^{**}=-\frac{B_2(0)}{B_3}$. However, computationally, the numerical value of $B_2(0)$ from equation (13) based on Table 1 is positive for $R_{0c}=1$.

Case 3. Suppose $R_{0c}<1$. Then $B_3,B_2(0),B_1(0)>0$. Therefore, it is clear there is no positive real root for $R_{0c}<1$.

Case 3 emanates from Theorem 3.6, since global stability of SARS-CoV-2 implies that no other equilibria exist. For ease of handling, we consider the case where $F(\alpha^{**})$ is linear with $B_1(0)=0$ and $B_2(0)=\Lambda\varphi H_0\Big[\theta+\gamma Y_2+\mu(1+\sum_{i=1}^{3}Y_i)\Big]$. The existence of a positive root of equation (12) is then reduced to the sign of $B_1(0)$ being negative, which occurs precisely at R_{0c} greater than unity. We then conclude with the following result.

Proposition 3.7. *The system (3) (for $\Omega = 0$) exhibits a unique positive endemic equilibrium if $R_{0c} > 1$ and no positive endemic equilibrium when $R_{0c} < 1$.*

Biologically, Proposition 3.7 implies that a stable SARS-CoV-2-free equilibrium does not co-exist with a stable endemic equilibrium.

In the following, we use the Centre Manifold Theory as in [34] to study the global asymptomatic stability of the full model when $\Omega \neq 0$. For the sake of uniformity, we let $S = x_1$, $V = x_2$, $L = x_3$, $I = x_4$, $Q = x_5$, $R = x_6$, $D = x_7$, $P = x_8$ such that $N = \sum_{i=1}^{7} x_i$. With the vector notation $x = (x_1, x_2, x_3, x_4, x_5, x_6, x_7, x_8)^T$, the system (3) in compact form is given by $\dot{x} = f(x)$, where $f = (f_1, f_2, f_3, f_4, f_5, f_6, f_7, f_8)^T$ is as follows:

$$\begin{cases} \dot{x}_1 = f_1 = \Lambda + \omega x_2 - c(1-\epsilon\phi)\dfrac{\eta_1 x_3 + \eta_2 x_4 + \eta_3 x_7 + \eta_4 x_8}{x_1 + x_2 + x_3 + x_4 + x_5 + x_6 + x_7} x_1 \\ \quad - (\mu + \nu_1)x_1, \\ \dot{x}_2 = f_2 = \nu_1 x_1 - c(1-\epsilon\phi)(1-\beta)\dfrac{\eta_1 x_3 + \eta_2 x_4 + \eta_3 x_7 + \eta_4 x_8}{x_1 + x_2 + x_3 + x_4 + x_5 + x_6 + x_7} x_2 \\ \quad - (\mu + \omega + \nu_2)x_2, \\ \dot{x}_3 = f_3 = c(1-\epsilon\phi)\dfrac{\eta_1 x_3 + \eta_2 x_4 + \eta_3 x_7 + \eta_4 x_8}{x_1 + x_2 + x_3 + x_4 + x_5 + x_6 + x_7}(x_1 + (1-\beta)x_2) \\ \quad - (\mu + \sigma + \theta)x_3, \\ \dot{x}_4 = f_4 = \sigma x_3 - (\mu + \xi + \delta_1)x_4, \\ \dot{x}_5 = f_5 = \xi x_4 - (\mu + \gamma + \delta_2)x_5. \\ \dot{x}_6 = f_6 = \nu_2 x_2 + \theta x_3 + \gamma x_5 - \mu x_6, \\ \dot{x}_7 = f_7 = \delta_1 x_4 + \delta_2 x_5 - \rho x_7, \\ \dot{x}_8 = f_8 = \Omega + d_1 x_3 + d_2 x_4 + d_3 x_7 - \varphi x_8, \end{cases} \tag{14}$$

The Jacobian of equation (14) at the SARS-CoV-2-free equilibrium, E_0 is given by

$$J(E_0) = \begin{pmatrix} -q_x & \omega & -n_p & -n_r & 0 & 0 & -m_p & -m_r \\ \nu_1 & -q_y & -n_q & -n_w & 0 & 0 & -m_q & -m_w \\ 0 & 0 & q_z & m_x & 0 & 0 & m_y & m_z \\ 0 & 0 & \sigma & -q_w & 0 & 0 & 0 & 0 \\ 0 & 0 & 0 & \xi & -q_n & 0 & 0 & 0 \\ 0 & \nu_2 & \theta & 0 & \gamma & -\mu & 0 & 0 \\ 0 & 0 & 0 & \delta_1 & \delta_2 & 0 & -\rho & 0 \\ 0 & 0 & d_1 & d_2 & 0 & 0 & d_3 & -\varphi \end{pmatrix}, \tag{15}$$

with $q_x = \mu + \nu_1$, $q_y = \mu + \omega + \nu_2$, $q_w = \mu + \xi + \delta_1$, $q_n = \mu + \gamma + \delta_2$, $n_p = c(1-\epsilon\phi)\eta_1 \frac{x_1^0}{N}$, $n_q = c(1-\epsilon\phi)(1-\beta)\eta_1 \frac{x_2^0}{N}$, $q_z = n_p + n_q - (\mu + \sigma + \theta)$, $n_r = c(1-\epsilon\phi)\eta_2 \frac{x_1^0}{N}$, $n_w = c(1-\epsilon\phi)(1-\beta)\eta_2 \frac{x_2^0}{N}$, $m_p = c(1-\epsilon\phi)\eta_3 \frac{x_1^0}{N}$, $m_q = c(1-\epsilon\phi)(1-\beta)\eta_3 \frac{x_2^0}{N}$, $m_r = c(1-\epsilon\phi)\eta_4 \frac{x_1^0}{N}$, $m_w = c(1-\epsilon\phi)(1-\beta)\eta_4 \frac{x_2^0}{N}$, $m_y = m_p + m_q$ and $m_z = m_r + m_w$.

We choose c as a bifurcation parameter. Therefore, if $R_{0c} = 1$, we obtain c^* as in equation (16)

$$c = (J_a J_b)^{-1} = c^*, \tag{16}$$

where

$$J_b = \frac{\eta_1}{(\mu+\sigma+\theta)} + \frac{\eta_2\sigma}{(\mu+\sigma+\theta)(\mu+\xi+\delta_1)} + \eta_3\sigma\frac{\xi\delta_2 + \delta_1(\mu+\gamma+\delta_2)}{(\mu+\sigma+\theta)(\mu+\xi+\delta_1)(\mu+\gamma+\delta_2)\rho} + \eta_4\frac{\rho(\mu+\gamma+\delta_2)\Big[d_1(\mu+\xi+\delta_1) + d_2\sigma\Big] + d_3\sigma\Big[\xi\delta_2 + \delta_1(\mu+\gamma+\delta_2)\Big]}{\varphi(\mu+\sigma+\theta)(\mu+\xi+\delta_1)(\mu+\gamma+\delta_2)\rho},$$

$$J_a = (1-\epsilon\phi)\frac{\mu H_0}{\mu(\mu+\omega+\nu_2) + \nu_1(\mu+\nu_2)}$$

At $c = c^*$, the Jacobian (15) has a simple zero eigenvalue since $A_0 = 0$ in equation (7), and all other eigenvalues are real and negative. This shows that E_0 is a non-hyperbolic point. On this basis, the Center Manifold Theory [35] can be used to analyze the system (3) near $c = c^*$. The right eigenvector $w = (w_1, w_2, w_3, w_4, w_5, w_6, w_7, w_8)^T$ associated with the zero eigenvalue of $J(E_0)$ manipulated at $c = c^*$ is

$$w_4 = \frac{\sigma}{q_w}w_3 = \pi_1 w_3, \quad w_5 = \frac{\xi\sigma}{q_n}w_3 = \pi_2 w_3,$$

$$w_7 = (\frac{\delta_1\pi_1 + \delta_2\pi_2}{\rho})w_3 = \pi_3 w_3,$$

$$w_8 = \frac{d_1 + d_2\pi_1 + d_3\pi_3}{\varphi}w_3 = \pi_4 w_3,$$

$$w_6 = \frac{\nu_2}{\mu}w_2 + \frac{\theta + \gamma\pi_2}{\mu}w_3 = \frac{\nu_2}{\mu}w_2 + \pi_5 w_3,$$

$$w_2 = -\frac{q_x\pi_6 + n_q + n_r\pi_1 + m_p\pi_3 + m_r\pi_4}{\frac{q_x q_y}{\nu_1} - \omega}w_3, \quad w_1 = \frac{q_y}{\nu_1}w_2 + \frac{\pi_6}{\nu_1}w_3,$$

and $w_3 = w_3 > 0$ with $\pi_6 = \frac{n_q + n_w\pi_1 + m_p\pi_3 + m_w\pi_4}{\nu_1}$.

In a similar fashion, we obtain the left eigenvector as follows;

$$v_1 = v_2 = v_6 = 0, \quad v_8 = \frac{m_z}{\varphi}v_3, \quad v_7 = \frac{m_y v_3 + d_3 v_8}{\rho}, \quad v_5 = \frac{\delta_2}{q_n}v_7,$$

$$v_4 = \frac{m_x v_3 + \xi v_5 + \delta_1 v_7 + d_2 v_8}{q_w},$$

and $v_3 = v_3 > 0$.

For the direction of the bifurcation, we determine the sign of the bifurcation parameters a and b. For a, one has

$$a = \sum_{k,i,j=1}^{8} v_k w_i w_j \frac{\partial^2 f_k}{\partial x_i \partial x_j}(E_0, c^*)$$

since $v_k = 0$, for $k = 1, 2, 6$. We shall concentrate on $k = 3, 4, 5, 7, 8$. Hence, the second partial derivatives at E_0 are as follows:

$$\frac{\partial^2 f_3}{\partial x_1 \partial x_3} = \frac{\partial^2 f_3}{\partial x_3 \partial x_1} = \frac{c^*(1-\epsilon\phi)\eta_1}{N}, \quad \frac{\partial^2 f_3}{\partial x_1 \partial x_4} = \frac{\partial^2 f_3}{\partial x_4 \partial x_1} = \frac{c^*(1-\epsilon\phi)\eta_2}{N},$$

$$\frac{\partial^2 f_3}{\partial x_1 \partial x_7} = \frac{\partial^2 f_3}{\partial x_7 \partial x_1} = \frac{c^*(1-\epsilon\phi)\eta_3}{N}, \quad \frac{\partial^2 f_3}{\partial x_1 \partial x_8} = \frac{\partial^2 f_3}{\partial x_8 \partial x_1} = \frac{c^*(1-\epsilon\phi)\eta_4}{N},$$

$$\frac{\partial^2 f_3}{\partial x_2 \partial x_3} = \frac{\partial^2 f_3}{\partial x_3 \partial x_2} = \frac{c^*(1-\epsilon\phi)(1-\beta)\eta_1}{N},$$

$$\frac{\partial^2 f_3}{\partial x_2 \partial x_4} = \frac{\partial^2 f_3}{\partial x_4 \partial x_2} = \frac{c^*(1-\epsilon\phi)(1-\beta)\eta_2}{N},$$

$$\frac{\partial^2 f_3}{\partial x_2 \partial x_7} = \frac{\partial^2 f_3}{\partial x_7 \partial x_2} = \frac{c^*(1-\epsilon\phi)(1-\beta)\eta_3}{N},$$

$$\frac{\partial^2 f_3}{\partial x_2 \partial x_8} = \frac{\partial^2 f_3}{\partial x_8 \partial x_2} = \frac{c^*(1-\epsilon\phi)(1-\beta)\eta_4}{N}.$$

Therefore,

$$a = 2v_3\Big[w_1 w_3 \frac{\partial^2 f_3}{\partial x_1 \partial x_3} + w_1 w_4 \frac{\partial^2 f_3}{\partial x_1 \partial x_4} + w_1 w_7 \frac{\partial^2 f_3}{\partial x_1 \partial x_7} + w_1 w_8 \frac{\partial^2 f_3}{\partial x_1 \partial x_8}\Big] + 2v_3\Big[w_2 w_3 \frac{\partial^2 f_3}{\partial x_2 \partial x_3} + w_2 w_4 \frac{\partial^2 f_3}{\partial x_2 \partial x_4} + w_2 w_7 \frac{\partial^2 f_3}{\partial x_2 \partial x_7} + w_2 w_8 \frac{\partial^2 f_3}{\partial x_2 \partial x_8}\Big]$$

from which we obtain

$$a = 2v_3\frac{c^*(1-\epsilon\phi)}{N}\Big[\eta_1 w_3 + \eta_2 w_4 + \eta_3 w_7 + \eta_4 w_8\Big]\Big[w_1 - \frac{F_x}{(\frac{q_x q_y}{\nu_1} - \omega)}(1-\beta)w_3\Big],$$

where

$$F_x = q_x\pi_6 + n_q + n_r\pi_1 + m_p\pi_3 + m_r\pi_4$$

But

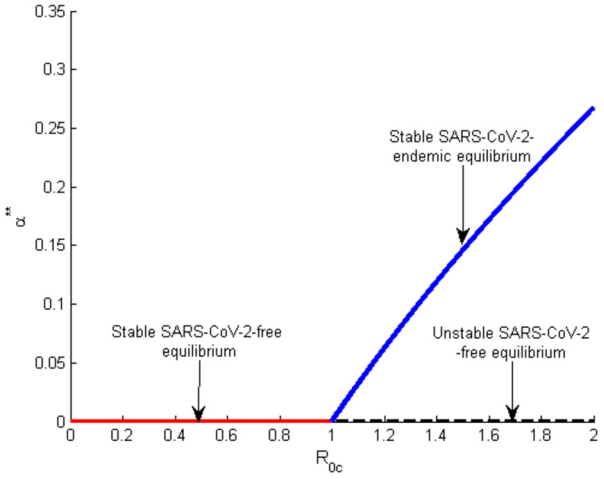

Fig. 2. Bifurcation diagram of the model system (3) for the special case ($\Omega = 0$). See Table 1 for the parameter values.

$$
\begin{aligned}
w_1 &= \frac{q_y}{\nu_1} w_2 + \pi_6 w_3 = -\frac{q_y F_x}{\nu_1} + \pi_6 w_3 \\
&= -\frac{q_x q_y \pi_6}{\nu_1(\frac{q_x q_y}{\nu_1} - \omega)} w_3 + \pi_6 w_3 - \frac{n_q + n_r\pi_1 + m_p\pi_3 + m_r\pi_4}{\frac{q_x q_y}{\nu_1} - \omega} w_3 \\
&= -\Big[\frac{q_x q_y \pi_6}{\nu_1(\frac{q_x q_y}{\nu_1} - \omega)} - \pi_6\Big] w_3 - \frac{n_q + n_r\pi_1 + m_p\pi_3 + m_r\pi_4}{\frac{q_x q_y}{\nu_1} - \omega} w_3 \\
&\leq -F_y w_3,
\end{aligned}
$$

where

$$
F_y = \frac{\pi_6 \omega \nu_1}{q_x q_y - \omega \nu_1} + \frac{n_q + n_r\pi_1 + m_p\pi_3 + m_r\pi_4}{\frac{q_x q_y}{\nu_1} - \omega}
$$

Hence,

$$
\begin{aligned}
a &\leq -2\upsilon_3 w_3^2 c^* \frac{(1-\epsilon\phi)}{N}\Big[\eta_1 + \eta_2\pi_1 + \eta_3\pi_3 + \eta_4\pi_4\Big]\Big[F_y + \frac{F_x}{(\frac{q_x q_y}{\nu_1} - \omega)}(1-\beta)w_3\Big] \\
&\leq 0
\end{aligned}
$$

For the bifurcation b, we have

$$
b = \sum_{k,j=1}^{8} \upsilon_k w_j \frac{\partial^2 f_k}{\partial x_j \partial c}(E_0, c^*) = \sum_{j=1}^{8} \upsilon_3 w_j \frac{\partial^2 f_3}{\partial x_j \partial c}(E_0, c^*)
$$

Recall that

$$
\begin{aligned}
\frac{\partial^2 f_3}{\partial x_3 \partial c^*} &= (1-\epsilon\phi)\eta_1(\frac{x_1^0}{N} + (1-\beta)\frac{x_2^0}{N}), \\
\frac{\partial^2 f_3}{\partial x_4 \partial c^*} &= (1-\epsilon\phi)\eta_2(\frac{x_1^0}{N} + (1-\beta)\frac{x_2^0}{N}), \\
\frac{\partial^2 f_3}{\partial x_7 \partial c^*} &= (1-\epsilon\phi)\eta_3(\frac{x_1^0}{N} + (1-\beta)\frac{x_2^0}{N}), \\
\frac{\partial^2 f_3}{\partial x_8 \partial c^*} &= (1-\epsilon\phi)\eta_4(\frac{x_1^0}{N} + (1-\beta)\frac{x_2^0}{N}),
\end{aligned}
$$

Therefore, b can be expressed as

$$
b = \upsilon_3(1-\epsilon\phi)\eta_1(\frac{x_1^0}{N} + (1-\beta)\frac{x_2^0}{N})\Big[\eta_1 w_3 + \eta_2 w_4 + \eta_3 w_7 + \eta_4 w_8\Big] > 0.
$$

Since $a < 0$ and $b > 0$, the system (3) does not exhibit the phenomena of backward bifurcation at $R_{0c} = 1$. For the fact that the direction of the bifurcation is forward as shown in Fig. 2, a stable SARS-CoV-2-free equilibrium can not co-exist with a stable endemic equilibrium. This is consistent with the result of [34], and hence, the following result is justified

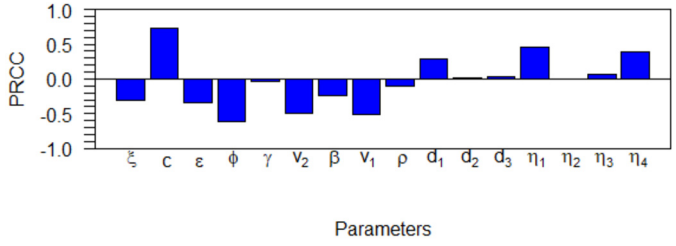

Fig. 3. COVID-19 sensitivities of R_{0c} with respect to the model parameters.

Theorem 3.8. *The unique SARS-CoV-2-endemic equilibrium of the system (3) is globally asymptomatically stable if $R_{0c} > 1$ and unstable otherwise.*

4. Sensitivity analysis

In this section, sensitivity analysis is conducted to show that each parameter in the system (3) considered is sensitive to the prevalence of COVID-19 pandemic. By way of definition, sensitivity index measures the relative change in a variable with respect to the relative change in the parameters involved. It is beneficial to determine the impact of the parameters on the effective reproduction number R_{0c}, which increases or decreases it the most for the sake of effective implementation of the proper control strategies needed to curtail the spread of the pandemic.

Definition 4.1. [36] The normalized forward sensitivity index of a variable J_υ with respect to parameter J_p is given by

$$
Z_p = \frac{\partial J_\upsilon}{\partial J_p} \times \frac{J_p}{J_\upsilon}
$$

Definition 4.2. [36] The sensitivity and elasticity of the effective reproduction number, R_{0c} with respect to a parameter, say c is given by

$$
Z_c^{R_{0c}} = \frac{\partial R_{0c}}{\partial c} \times \frac{c}{R_{0c}}
$$

With the Definition 4.2 and partial rank correlation coefficient (PRCC), the sensitivity indices obtained using the estimated parameter values in Table 1 are depicted in Fig. 3.

The positivity of the sensitivity indices of the parameters of the effective reproduction number indicate that 10% increment in all the parameter values may lead to an increase in the reproduction number of the pandemic. As illustrated in Fig. 3, the contact rate c is the highest, and the most sensitive parameter. This means that an increase (or a decrease) of the values of c will increase (or decrease) R_{0c} by 80%. However, of all the negative indices illustrated in Fig. 3. the public health advocacy compliance rate, ϕ is the most sensitive parameter followed by the primary and booster doses of COVID-19 vaccine. This implies that an increase (or a decrease) of the value of ϕ, ν_1 and ν_2 will decrease or increase R_{0c} by 60%, 50% and 40% respectively. Hence, for the parameter values used, an increase in the compliance rate by at least 70% to public health policies of wearing face masks in public places, maintaining social distancing, regular washing of hands, vaccination, proper burial (particularly in Africa) etc. could drag the pandemic to extinction and consequently leads to herd immunity since $R_{oc} = 0.833302892 < 1$ at $\phi = 0.7$. But, it was found that if 60% of the constituents followed the optimal control guidelines, then the pandemic will remain persistent in the population since $R_{oc} = 1.03603225 > 1$ at $\phi = 0.6$. However, an increase in parameters with positive sensitivity indices of R_{0c} will result in high prevalence of COVID-19. This calls for appropriate controls to be adopted by the public health administrators in order to stop the spread of COVID-19 in the human and environmental host populations. Specifically, we recommend that to achieve optimal compliance to COVID-19 public health policies, the government at all levels should enforce sanctions on constituents who failed to adhere strictly

to COVID-19 protocols. In addition, testing and vaccination of the populace for COVID-19 should be a necessary criterion for assessing some basic social needs. This recommendation becomes imperative as a result of the unwillingness of most constituents in Africa (particularly Nigeria) in availing themselves for testing and vaccination and adhering to COVID-19 protocols.

5. Optimal control model

In this section, we are interested in examining the optimal strategies of ending COVID-19 pandemic. This is possible by introducing the following controls to the model (3)

u_1: Prevention strategy aimed at inhibiting the total virus transmission from latent, infected, dead bodies and pathogens via public health advocacy for anti-open defecation, social distancing and wearing of face masks in public places
u_2: Booster vaccine control program targeted at ensuring that primary vaccinated people attain herd immunity to COVID-19 pandemic
u_3: Intense medical care through isolation for the infected people
u_4: Disinfecting or fumigating of surfaces and dead bodies before burial to avoid environmental transmission.

Thus, the optimal control system now reads:

$$\begin{aligned}
\frac{dS(t)}{dt} &= \Lambda + \omega V - c(1-g_1u_1(t))\Big(\frac{\eta_1 L+\eta_2 I+\eta_3 D+\eta_4 P}{N}\Big)S \\
&\quad -(\mu+\nu_1)S, \\
\frac{dV(t)}{dt} &= \nu_1 S-(1-\beta)c(1-g_1u_1(t))\Big(\frac{\eta_1 L+\eta_2 I)+\eta_3 D+\eta_4 P}{N}\Big)V \\
&\quad -(\mu+\omega+\nu_2)V-g_2u_2(t)V, \\
\frac{dL(t)}{dt} &= c(1-g_1u_1(t))\Big(\frac{\eta_1 L+\eta_2 I+\eta_3 D+\eta_4 P}{N}\Big)\Big(S+(1-\beta)V\Big) \\
&\quad -(\mu+\sigma+\theta)L, \\
\frac{dI(t)}{dt} &= \sigma L-\Big(\mu+\xi+\delta_1\Big)I-g_3u_3(t)I, \\
\frac{dQ(t)}{dt} &= \xi I+g_3u_3(t)I-\Big(\mu+\gamma+\delta_2\Big)Q. \\
\frac{dR(t)}{dt} &= \nu_2 V+g_2u_2(t)V+\theta L+\gamma Q-\mu R, \\
\frac{dD(t)}{dt} &= \delta_1 I+\delta_2 Q-\rho D-g_4u_4(t)D, \\
\frac{dP(t)}{dt} &= \Omega+d_1 L+d_2 I+d_3 D-\varphi P-g_4u_4(t)P,
\end{aligned} \tag{17}$$

subject to the initial conditions $S(0)=S_0,\ V(0)=V_0,\ L(0)=L_0,\ I(0)=I_0,\ Q(0)=Q_0,\ R(0)=R_0,\ D(0)=D_0,\ P(0)=P_0$.
And the objective functional which is linearly and quadratically defined as follows

$$J(u_1,u_2,u_3,u_4)=\int_0^T\Big[b_1L(t)+b_2I(t)+b_3D(t)+b_4P(t)+\sum_{i=1}^{4}\frac{h_i}{2}u_i^2\Big]dt, \tag{18}$$

where T is the final time for complete implementation of the controls, $b_i, i=1,2,3,4$ are positive constants, and $h_i, i=1,2,3,4$ are weight constants for the interventions and treatment against the spread of COVID-19. Note that T can be chosen taking into consideration the time interval between primary vaccine series and booster dose(s) of COVID-19 which might take at least 5 months (less than a year) [37]. The period for the treatment and the recovery of an infected person is also key for the choice of T. Also, when $u_i=0$ in equation (18), the dynamics of the epidemiological system remain populated with infected persons and COVID-19 pathogens. Hence, the disease continues to increase after T. The linear and quadratic form of the controls in (18) and in the objective functional enable the minimization of the Hamiltonian function corresponding to the equation (20). The expression $\frac{h_iu_i^2}{2}$ represents the costs associated with u_i. The term is quadratic because, it is mathematically manageable and to avoid the problems of chattering control usually associated with algebraically simpler linear terms [38]. Thus, the greater values of h_i indicate higher cost of implementing the controls u_i. Note that g_1, g_2, g_3 and g_4 quantifies the usefulness of the optimal controls $u_1(t), u_2(t), u_3(t)$ and $u_4(t)$ respectively in equation (17). Also, $u_i(t)=0$ means no response to the control i and $u_i(t)=1$ means complete response to the control i. Thus, using the Pontryagin's Maximum Principle as in [21] we obtain an optimal control $(u_1^*,u_2^*,u_3^*,u_4^*)\in U$ such that equation (19) is satisfied

$$J(u_1^*,u_2^*,u_3^*,u_4^*)=min\Big\{J(u_1,u_2,u_3,u_4)\mid(u_1,u_2,u_3,u_4)\in U\Big\}, \tag{19}$$

with the following pseudo-Hamilton

$$H=b_1L(t)+b_2I(t)+b_3D(t)+b_4P(t)+\sum_{i=1}^{4}\frac{h_i}{2}u_i^2+\sum_{i=1}^{8}\lambda_iy_i, \tag{20}$$

where y_i is the ith right hand side of (17) and λ_i is the ith adjoint that uphold the co-state functions

$$\begin{aligned}
\lambda_1' &= -\frac{\partial H}{\partial S}, \quad \lambda_2' = -\frac{\partial H}{\partial V}, \quad \lambda_3' = -\frac{\partial H}{\partial L}, \quad \lambda_4' = -\frac{\partial H}{\partial I}, \\
\lambda_5' &= -\frac{\partial H}{\partial Q}, \quad \lambda_6' = -\frac{\partial H}{\partial R}, \quad \lambda_7' = -\frac{\partial H}{\partial D}, \quad \lambda_8' = -\frac{\partial H}{\partial P},
\end{aligned} \tag{21}$$

where the detailed form of (21) is given by equation (22)

$$\begin{aligned}
\lambda_1' &= (\lambda_1-\lambda_3)(1-g_1u_1)\alpha_0+(\lambda_1-\lambda_2)\nu_1+\lambda_1\mu, \\
\lambda_2' &= (\lambda_2-\lambda_3)(1-\beta)(1-g_1u_1)\alpha_0+(\lambda_2-\lambda_6)(\nu_2+g_2u_2)+(\lambda_2-\lambda_1)\omega+\lambda_2\mu, \\
\lambda_3' &= -b_1+c(\lambda_1-\lambda_3)(1-g_1u_1)\eta_1\frac{S}{N}+c(\lambda_2-\lambda_3)(1-g_1u_1)(1-\beta)\eta_1\frac{V}{N} \\
&\quad +(\lambda_3-\lambda_4)\sigma+(\lambda_3-\lambda_6)\theta-\lambda_8d_1+\lambda_3\mu, \\
\lambda_4' &= -b_2+c(\lambda_1-\lambda_3)(1-g_1u_1)\eta_2\frac{S}{N}+c(\lambda_2-\lambda_3)(1-g_1u_1)(1-\beta)\eta_2\frac{V}{N} \\
&\quad +(\lambda_4-\lambda_5)(\xi+g_3u_3)+(\lambda_4-\lambda_7)\delta_1-\lambda_8d_2+\lambda_4\mu, \\
\lambda_5' &= (\lambda_5-\lambda_6)\gamma+(\lambda_5-\lambda_7)\delta_2+\lambda_5\mu, \\
\lambda_6' &= \lambda_6\mu, \\
\lambda_7' &= -b_3+c(\lambda_1-\lambda_3)(1-g_1u_1)\eta_3\frac{S}{N}+c(\lambda_2-\lambda_3)(1-g_1u_1)(1-\beta)\eta_3\frac{V}{N} \\
&\quad +\lambda_7(\rho+g_4u_4)-\lambda_8d_3, \\
\lambda_8' &= -b_4+c(\lambda_1-\lambda_3)(1-g_1u_1)\eta_4\frac{S}{N}+c(\lambda_2-\lambda_3)(1-g_1u_1)(1-\beta)\eta_4\frac{V}{N} \\
&\quad -\lambda_8(\varphi+g_4u_4).
\end{aligned} \tag{22}$$

with the final conditions $\lambda_i(T), i=1,2,...,8$. The necessary and sufficient optimality conditions are given by equation (23)

$$\frac{\partial H}{\partial u_1^*}=0, \quad \frac{\partial H}{\partial u_2^*}=0, \quad \frac{\partial H}{\partial u_3^*}=0, \quad \frac{\partial H}{\partial u_4^*}=0, \tag{23}$$

which subsequently resulted in the optimal controls in equation (24)

$$\begin{aligned}
u_1^* &= max\Big\{0,min\Big(1,\frac{\Big((\lambda_3-\lambda_1)S+(\lambda_3-\lambda_2)(1-\beta)V\Big)cg_1\alpha_0}{h_1}\Big)\Big\}, \\
u_2^* &= max\Big\{0,min\Big(1,\frac{(\lambda_2-\lambda_6)g_2V}{h_2}\Big)\Big\}, \\
u_3^* &= max\Big\{0,min\Big(1,\frac{(\lambda_4-\lambda_5)g_3I}{h_3}\Big)\Big\}, \\
u_4^* &= max\Big\{0,min\Big(1,\frac{(\lambda_7D+\lambda_8P)g_4}{h_4}\Big)\Big\},
\end{aligned} \tag{24}$$

where

$$\alpha_0=\Big(\frac{\eta_1L+\eta_2I+\eta_3D+\eta_4P}{N}\Big).$$

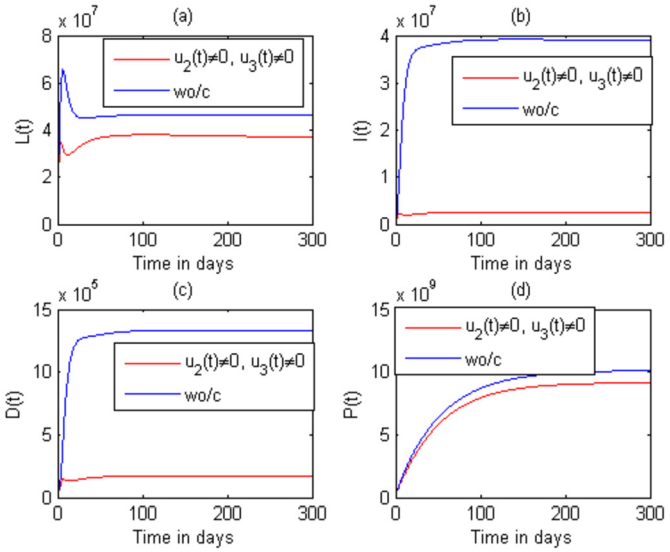

Fig. 4. Dynamics of (a) latent, (b) infectious, (c) dead bodies and (d) corona virus pathogens using strategy A. Note that wo/c represents without control.

6. Numerical simulations

In this section, we backup the analytical results by simulating the optimal control system using Runge-Kutta forward-backward method coded in Matlab and the estimated parameters in Table 1 with the initial values $S(0) = 199,419,568$, $V(0) = 734,764$, $L(0) = 2,806,333$, $I(0) = 201,798$, $Q(0) = 3,019,336$, $R(0) = 2,655$, $D(0) = 190,563$, $P(0) = 211,924,782$ and $N(0) = 212,375,017$ estimated from COVID-19 cases in Nigeria. The weight constants used include $h_1 = 0.12$, $h_2 = 0.4$, $h_3 = 2$, $h_4 = 0.15$ and $b_1 = b_2 = b_3 = b_4 = 1$. These weights constants are chosen based on the cost of implementing the controls as reported in [25]. That is, the cost of public health advocacy is lower than the cost of disinfecting or fumigating of surfaces and dead bodies ($h_1 < h_4$). The cost of the latter is in turn less expensive than booster vaccine ($h_4 < h_2$) while the cost of treating isolated people tends to be higher than the rest ($h_1 < h_4 < h_2 < h_3$). To assess the impact of various controls to curbing the spread of COVID-19, the following combinations scenarios are selected.

1. Strategy A: COVID-19 prevention via booster vaccine + medical care (isolation program) ($u_2 \neq 0,\ u_3 \neq 0$)
2. Strategy B: COVID-19 prevention via booster vaccine + fumigating of surfaces and dead bodies ($u_2 \neq 0,\ u_4 \neq 0$)
3. Strategy C: Medical care (isolation program) + fumigating of surfaces and dead bodies ($u_3 \neq 0,\ u_4 \neq 0$)
4. Strategy D: COVID-19 prevention via booster vaccine + medical care (isolation program) + fumigating of surfaces and dead bodies ($u_2 \neq 0,\ u_3 \neq 0,\ u_4 \neq 0$)
5. Strategy E: Public health advocacy + booster vaccine + medical care (isolation program) + fumigating of surfaces and dead bodies ($u_1 \neq 0,\ u_2 \neq 0,\ u_3 \neq 0,\ u_4 \neq 0$)

For all the above strategies, the effective reproductive number computed using parameter values in Table 1 is $R_{0c} = 1.03603225 > 1$.

6.1. Discussion and limitations

6.1.1. Strategy A

In this strategy, the combination of booster vaccine program (u_2) and intense medical care (isolation program) (u_3) is used without fumigation of surfaces and dead bodies ($u_4 = 0$). The dynamics of latent COVID-19, Infectious, dead bodies and corona virus pathogens are given in Fig. 4. Figs. 4(a) and 4(b) show that booster vaccine and isolation for latent and infected COVID-19 controls provide a significant reduction in latent COVID-19 and infectious populations compared to having no controls. Similar scenarios were also observed in the dynamics of the dead and pathogens which is lower as compared to the situation when implemented without controls in Figs. 4(c) and 4(d). This result is consistent with the outcome as in the work of [25]. We noted however in Figs. 4(a)- 4(c) that the infected compartments (Latent and infectious) turn to be stable after 50 days. Thus, the number of death cases after 50 days remains constant through out. The profile of optimal controls u_2^* and u_3^* is depicted in Fig. 5. Booster vaccine program and isolation could be implemented intensively for 300 days before declining. This strategy however lacks the capacity to curtail the pandemic completely as the result shows in Fig. 4.

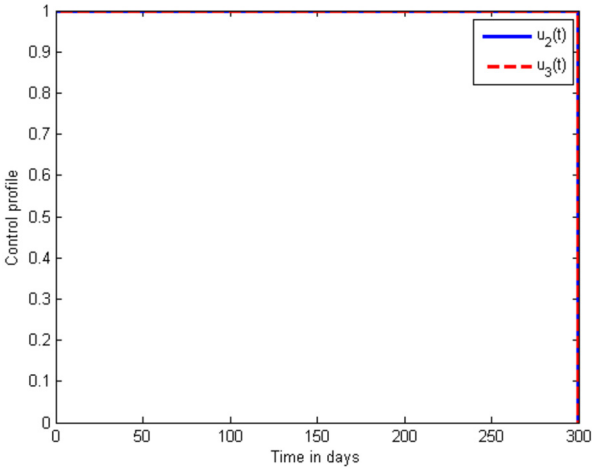

Fig. 5. Profile of optimal controls u_2^* and u_3^* for strategy A.

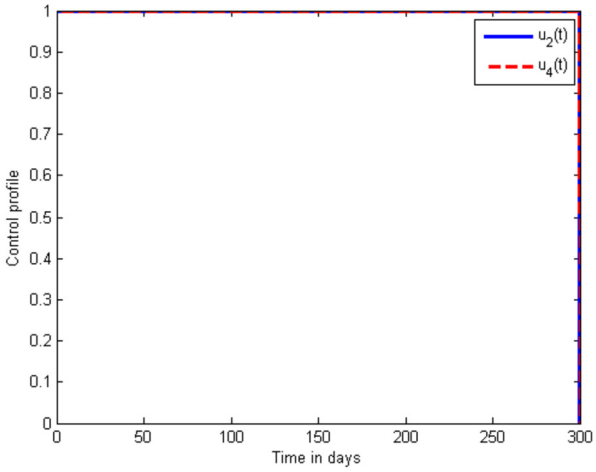

Fig. 6. Profile of optimal controls u_2^* and u_4^* for strategy B.

6.1.2. Strategy B

In the strategy B, the optimal controls for COVID-19 prevention (u_2) and fumigation of surfaces and dead bodies (u_4) are used. The profile of the optimal controls (u_2^*) and (u_4^*) is given in Fig. 6. With this strategy, booster vaccine and fumigation intervention mechanisms could be intensively implemented for 300 days before decreasing at day 300. The dynamics of the dead, COVID-19 pathogens, latent and infectious people is depicted in Fig. 7. Strategy B reduces significantly the COVID-19 pathogens from the environment and the number of death cases to the bearest minimum as illustrated in Figs. 7c and 7d. Consequently, this drags both the latent and infectious people to almost extinction as compared with the absence of the controls as explained by Figs. 7a and

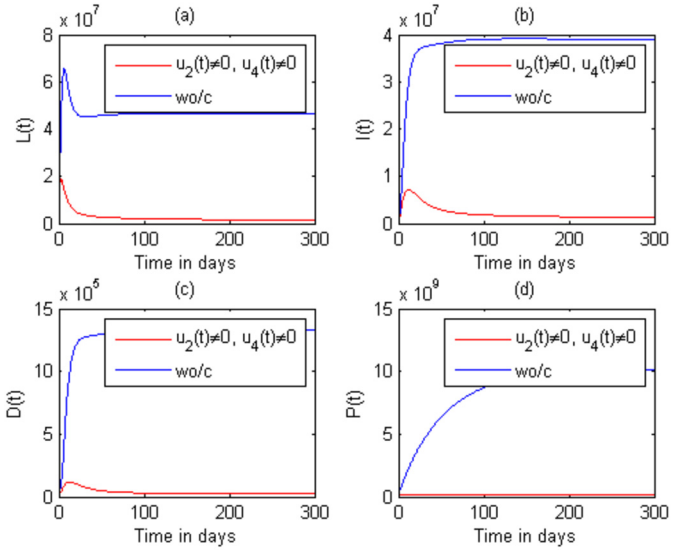

Fig. 7. Dynamics of (a) latent, (b) infectious, (c) dead bodies and (d) corona virus pathogens using strategy B. Note that wo/c represents without control.

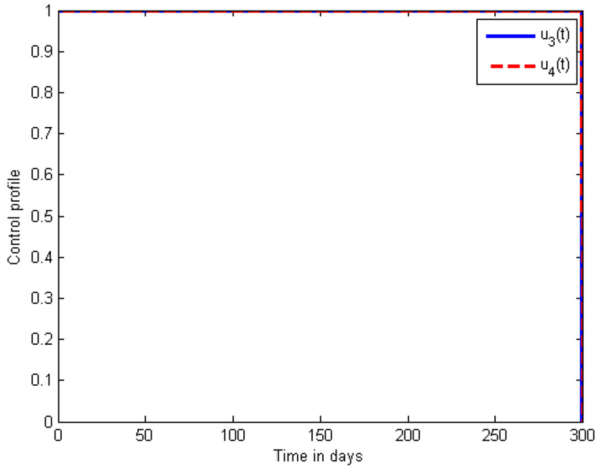

Fig. 8. Profile of optimal controls u_3^* and u_4^* for strategy C.

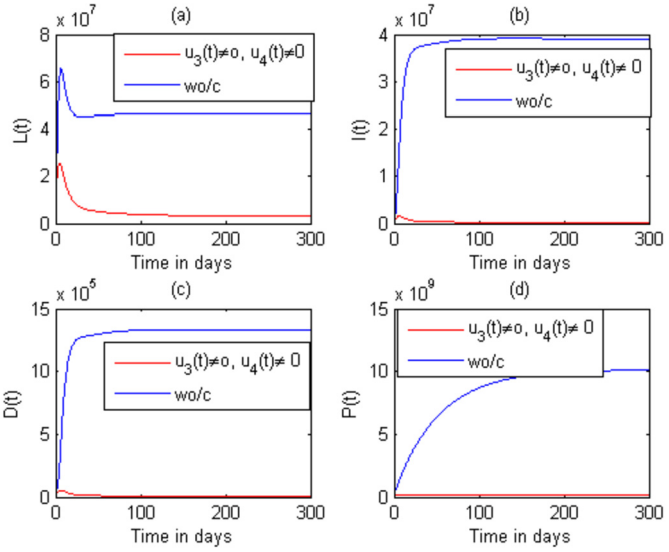

Fig. 9. Dynamics of (a) latent, (b) infectious, (c) dead bodies and (d) corona virus pathogens using strategy C. Note that wo/c represents without control.

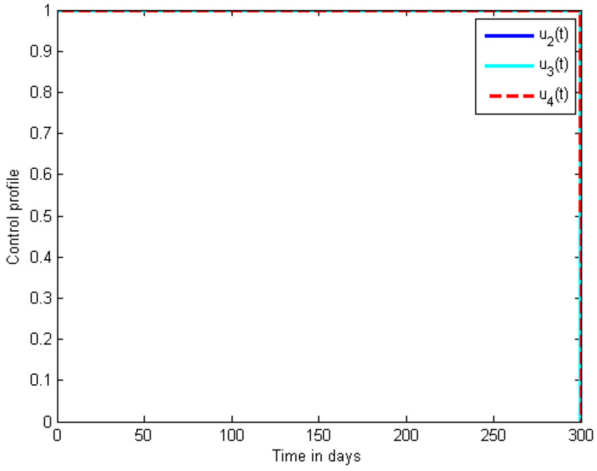

Fig. 10. Profile of optimal controls u_2^*, u_3^* and u_4^* for strategy D.

7b. This result is promising in mitigating COVID-19 pandemic just as in the work of [39]. However, precautionary measures during fumigation should be put in place because misuse of disinfectants can pose threat to the living beings and environment as reported in [40, 41]. Furthermore, we suggest that open defecation and improper burial practices common to African settings be discouraged in order to reduce the population of COVID-19 pathogens in the environment. So far, strategy B could be preferred to strategy A since it eradicates COVID-19 from human population.

6.1.3. Strategy C

In strategy C, the combination of isolation control (u_3) and fumigation of surfaces and dead bodies (u_4) is implemented. The control profile of strategy C is depicted in Fig. 8. Here, we observed that isolation and fumigation controls could be optimally implemented at 300 days before deceasing at day 300. Fig. 9 shows the dynamics of infected (both latent and infectious) people, dead bodies and pathogens with respect to the controls u_3 and u_4. We noticed from Fig. 9 (b-d) that the isolation and fumigation strategy could reduce the total number of infectious people to zero after 80 days and end the death sentence due to COVID-19 in about 50 days even though certain pathogenic elements of the virus may remain in the environment. The latently infected people as seen in Fig. 9a reduces steadily and becomes stable asymptotically upon the implementation of this strategy than when no controls are available. This strongly agrees with the result recently published by [39].

6.1.4. Strategy D

In this strategy, a combination of COVID-19 prevention via booster vaccine program (u_2), isolation (u_3) and disinfection/fumigation of surfaces and dead bodies (u_4) are adopted concurrently. The profile of the strategy D is given in Fig. 10. This strategy can be executed maximally within 300 days and then decreases as illustrated in Fig. 10. Fig. 11 shows the dynamics of infected (latent and infectious), dead bodies and pathogens in the presence of triple control strategies. This strategy indeed significantly ends the dead cases due to COVID-19 in about 20 days as in Fig. 11c. It stabilizes the growth of the virus in the environment within the first 290 days in Fig. 11d and eliminates the infectious people completely in the population after 20 days of implementation as seen in Fig. 11b. As in strategy B, the latently infected people are reduced and became stable asymptotically in Fig. 11a. A contrary outcome is expected when there are no such controls.

6.1.5. Strategy E

Here, we implement the combination of public health advocacy policies and booster vaccine inclusive ($u_1(t), u_2(t)$), isolation ($u_3(t)$ and

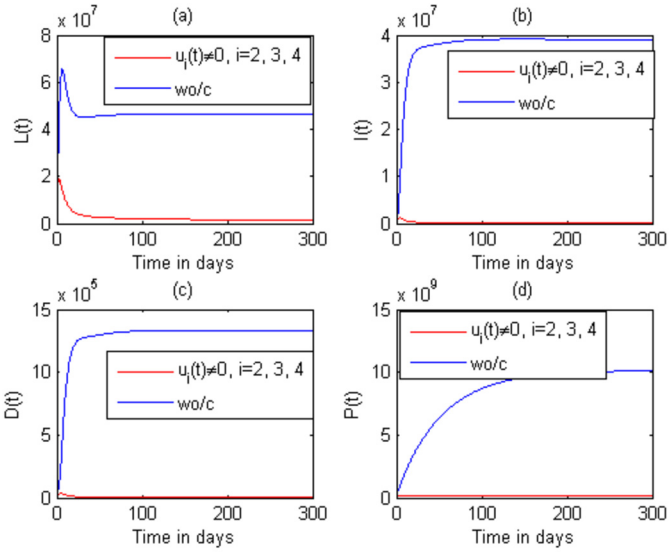

Fig. 11. Dynamics of (a) latent, (b) infectious, (c) dead bodies and (d) corona virus pathogens using strategy D. Note that wo/c represents without control.

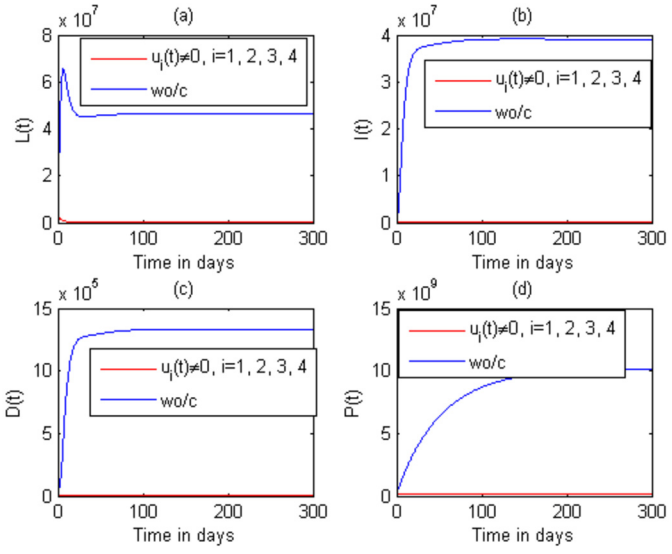

Fig. 12. Dynamics of (a) latent, (b) infectious, (c) dead bodies and (d) corona virus pathogens using strategy E. Note that wo/c represents without control.

disinfecting of surfaces and dead bodies $u_4(t)$ to obtain Fig. 12 and the control profile in Fig. 13.

We saw from Figs. 12b and 12c that after the implementation of strategy E, infectious people and the dead are entirely eliminated from the population. This control strategy dragged the latent individuals to zero after 10 days in Fig. 12a. However, it was observed from Fig. 12d that certain quantum of the virus remains constantly in the environment. The persistence of COVID-19 pathogens as observed in Figs. 4, 7, 9 and 12 could be as a result of uncertainties surrounding the source of the virus as claimed by assumption 6. This result is unique and needs medical follow-up to end the COVID-19 burdens.

In the next numerical experiments, we did the comparisons of single controls and these strategies A, B, C, D, and E on the dead, corona pathogens, latent and infectious people as depicted in the Figs. 14 and 15. Optimal public health advocacy, booster vaccine, isolation and fumigation of surfaces and dead bodies as demonstrated in Fig. 14 (a-d) have substantial reduction in all state solutions when compared to singular controls scenarios. However, for a singular strategy preference, booster vaccine is better for human population while fumigation is

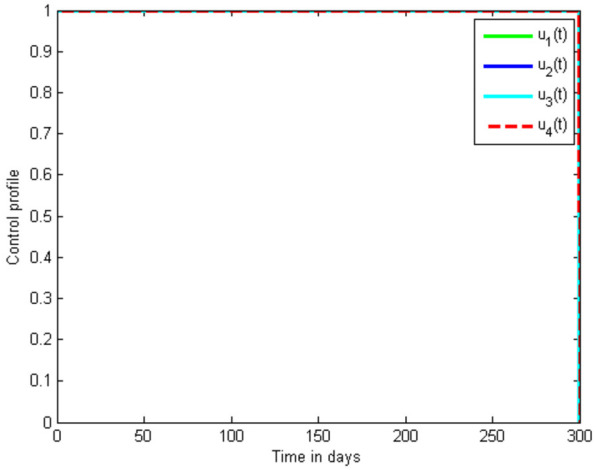

Fig. 13. Profile of optimal controls u_1^*, u_2^*, u_3^* and u_4^* for strategy E.

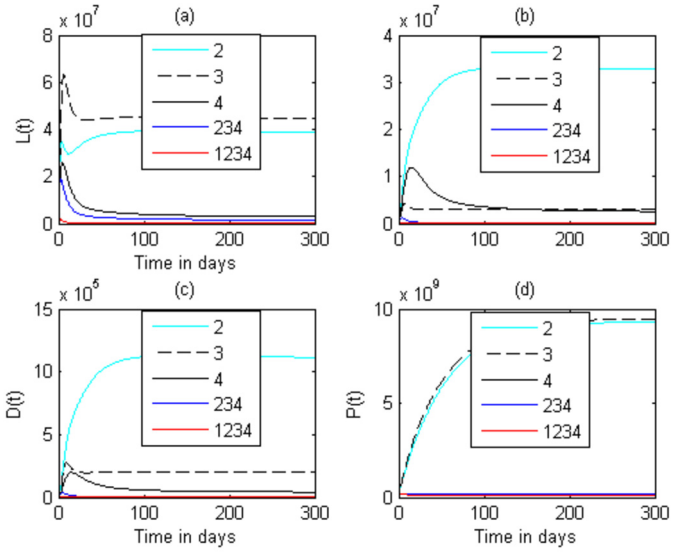

Fig. 14. Comparisons of the corresponding to latently infected (*a*), infectious (*b*), dead bodies (*c*) and corona virus pathogens (*d*) with the application of control strategies (single controls, strategy D (234) and strategy E (1234)).

the desired approach for corona virus clearance in the environment as observed in the result of [39]. On the other hand, despite the high positive influence of strategy E on the prevalence of the disease in Fig. 15 (a-d), strategies C and D also reduce substantially, the number of infected populations and viruses from the surrounding thereby reducing the COVID-19 burden and mortality cases. It is obvious that in the absence of interventions, the number of infected and death cases remain high with respect to the increase in concentration of the viruses in the environment. On the contrary, strategy A even though may be necessary but not sufficient enough in ending COVID-19 pandemic as clearly shown in Fig. 15 (a-d).

For the fact that models of COVID-19 are not sufficiently developed, future works can be derived from the limitations of this paper in the following areas:

i. The multiple strains setting to cater for the difficult scenario where a region is invaded by more than one corona virus strains.
ii. The use of other incidence functions such as Holling type functions for the environment-to-human transmission.
iii. Assess the cost-effectiveness of each of the control strategies in the study.

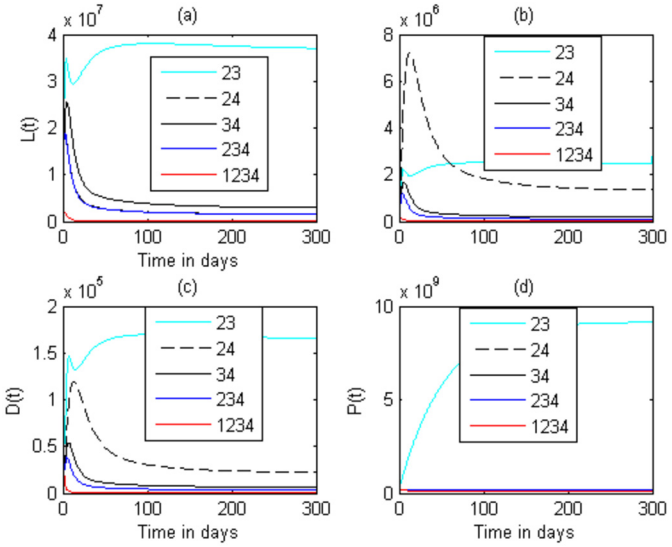

Fig. 15. Comparisons of the corresponding to latent infected (*a*), symptomatic infected (*b*), dead bodies (*c*) and corona virus pathogens (*d*) with the application of control strategies (strategy A (23), strategy B (24), strategy C (34), strategy D (234) and strategy E (1234)).

iv. The extension of the model to cater for the complex ecology of the corona virus transmission.
v. Modelling of SARS-CoV-2 dynamics with transmission kinetics that requires a smooth or strict threshold of Hill function type.
vi. Further theoretical results on equilibria analysis (where the constant inflow of corona virus into the environment is not suspended, $\Omega > 0$ in equation (11)) can be explored.

7. Conclusion

The spread of corona virus in Nigeria and other parts of the world has been relatively more studied in the human-to-human transmission ([16, 17, 18, 19, 20, 21]) than in the indirect environmental (environment-to-human-to-environment) transmission route. In this paper, we targeted the latter route, which is the main characteristics that surrounds the misery of the outbreak of corona virus. Instead of dealing with only direct transmission, we formulated and analyzed a deterministic compartmental model for the transmission dynamics of corona virus, that enriched the classical SIR model with three additional compartments of vaccinated individuals, dead bodies and free-living corona virus pathogens with vital dynamics and booster vaccine impact. In this dual setting of human-to-human and environment-to-human-to-environment transmission, we recorded our main contributions into three perspectives.

From the theoretical perspective, we have shown that the endemicity of the pandemic increases with the recruitment of corona virus pathogens and shedding from the latent, infectious and dead bodies; and that the disease vanishes out in the absence of such recruitments. The full model is proved to be well-posed. For the model without the recruitment of corona virus ($\Omega = 0$), the SARS-C0V-2-free equilibrium has a stable global asymptotic behaviour when $R_{0c} < 1$ and unstable if otherwise. Using the Center Manifold Theory, the coexistence of SARS-CoV-2-free and endemic equilibria is not guaranteed for the full model with $\Omega > 0$. Hence, the endemic equilibrium of the full model is globally asymptotically stable whenever $R_{0c} > 1$.

From the sensitivity point of view, the study revealed that shedding, transmission parameters and contacts made are very influential in the increase of the ongoing COVID-19 pandemic cases. Based on the parameters values in Table 1, further results suggest that if at least 70% of the constituents followed the public health policies of wearing of masks, maintaining social distancing, regular washing of hands, testing and vaccination of populace for COVID-19, proper burial (particularly in Africa) could help in attaining herd immunity. However, this outcome may not always be true as model parameters are known with more certainty. Thus, to achieve the above, we recommend that: (1) government at all levels should enforce sanctions on constituents who failed to adhere strictly to COVID-19 protocols, and (2) testing and vaccination of the populace for COVID-19 should be a necessary criterion for assessing some basic social needs.

Pontryagin's Maximum Principle is adopted to solve for the necessary conditions for the optimal values of the controls that minimizes the spread of the pandemic. The results from the optimal control problem revealed that the pandemic may be brought under check by implementing continuous controls within a short period of time, indicating that optimal control strategy is effective in human and environment. Specifically, strategy E for implementing the public health advocacy, booster vaccine program, treatment of isolated people and disinfecting or fumigating of surfaces and dead bodies before burial is found to be the most effective strategy in curbing the spread of the disease. However, control policies implementing either of the strategies (A-D) presented in this study could also be helpful in infection reduction and mortality control. In as much as the optimal control strategies in this study portray, it is worth investigating in the future, the cost-benefits of the aforementioned controls for better economic assessment. It should also be noted that since the main source for SARS-CoV-2 is still under scientific investigations, other future studies may model the recruitment rate of the virus as time dependent function. This we hope will add greater value to control strategies for curbing the disease.

Declarations

Author contribution statement

N.I. Akinwande, T.T. Ashezua: Conceived and designed the analysis. R.I. Gweryina: Conceived and designed the analysis; wrote the paper. S.A. Somma, F.A. Oguntolu, O.N. Abdurrahman, T.P. Adajime, S. Abdulrahman: Analyzed and interpreted the data. A. Usman, F.S. Kaduna, F.A. Kuta, R.O. Olayiwola, A.I. Enagi, G.A. Bolarin, M.D. Shehu: Contributed analysis tools or data.

Funding statement

N.I. Akinwande was supported by Tertiary Education Trust Fund [TETF/ES/DR&D-CE/NRF2020/SETI/82/VOL.1].

Data availability statement

Data included in article/supp.material/referenced in article.

Declaration of interests statement

The authors declare no conflict of interest.

Additional information

No additional information is available for this paper.

Acknowledgements

We sincerely appreciate our various institutions for the conducive academic environment for the pursuit of the research. The authors are grateful to the editor and the anonymous reviewers for their invaluable comments and constructive criticisms, which have improved the manuscript.

References

[1] WHO, WHO-convened global study of origins of SARS-CoV-2 retrieved on 14 Jan. to 10 Feb. 2021, from https://www.who.int/health-topics/coronavirus/origins-of-the-virus.

[2] WHO, COVID-19 weekly epidemiological update on COVID-19 retrieved on 13 October 2021, from https://www.who.int/publications/m/item.

[3] Nigeria Centre for Disease Control (NCDC), COVID-19 Nigeria. Retrieved on Tuesday July 19, 2022 from https://covid19.ncdc.gov.ng/.

[4] WHO, Transmission of SARS-CoV-2: implications for infection prevention precautions, retrieved from https://www.who.int/news-room/commentators/details/transmission, 2020.

[5] M. Gabbrielli, C. Gandolfo, G. Anichini, T. Candelori, M. Benvenuti, G.G. Savellini, M.G. Cusi, How long can SARS-CoV-2 persist in human corpses?, Int. J. Infect. Dis. 106 (2021) 1–2.

[6] R.S. Quilliam, V. Moresco, M. Weidmann, H. Roxburgh, COVID-19: the environmental implications of shedding SARS-CoV-2 in human faeces, Environ. Int. 140 (2020) 105790.

[7] N.R. Singh, Funeral practices with dead bodies of Covid-19 infected patients, scientific modifications needed in who's recommendations, CIBTech J. Microbiol. 9 (2020) 1–6.

[8] F.D. Gennaro, D. Pizzol, C. Marotta, M. Antunes, V. Racalbuto, N. Veronese, L. Smith, Coronavirus disease current status and future perspectives: a narrative review, Int. J. Environ. Res. Public Health 17 (2020).

[9] Centers for Disease Control and Prevention (CDC), Overview for testing for SArs-CoV-2 (Covid-19). Retrieved on tuesday oct. 19, 2021 from https://www.cdc.gov > hep > testing.

[10] WHO, Coronavirus disease 2019 (Covid-19) situation report-51, retrieved on monday January 7, 2022 from https://www.who.int/publications/m/item/situation-report-51.

[11] WHO, Vaccine efficacy, effectiveness and protection, retrieved from https://www.who.int/news-room/feature-stories/vaccine-efficacy-effectiveness-and-protection, 2021, on friday Oct. 15, 2021.

[12] Centers for Disease Control and Prevention (CDC), Covid-19 vaccine breakthrough infections reported to CDC- United States, Jan 1–April 30, 2021, https://stacks.cdc.gov, 2021.

[13] X. Deng, M. Evdokimova, A. O'Brien, C.I. Rowe, N.M. Clark, A. Harrington, G.E. Reid, S.I. UpRichard, S.C. Baker, Breakthrough infections with multiple lineages of sars-cov-2 variants reveals continued risk of severe disease in immunosuppressed patients, Viruses 13 (9) (2021) 1743.

[14] Centers for Disease Control and Prevention (CDC), COVID-19 vaccine booster shots. Retrieved on June 25, 2022 from https://www.cdc.gov/coronavirus/2019.ncov/vaccines/booster-shots.html~(2022).

[15] National Institute for Health (NIH), Lasting immunity found after recovery from Covid-19. Retrieved on June 25, 2022 from https://www.nih.gov/news-events/nih-retreat-matters/lasting-immunity-found-after-recovery-from-covid-19, 2021.

[16] A.B. Gumel, E.A. Iboi, C.N. Ngonghala, E.H. Elbasha, A primer on using mathematics to understand COVID-19 dynamics: modelling, analysis and simulations, Infect. Dis. Model. 6 (2021) 148–168.

[17] A.I. Abioye, J.P. Olumuyiwa, H.A. Ogunseye, F.A. Oguntolu, K. Oshinubi, A.A. Ibrahim, I. Khan, Mathematical model of COVID-19 in Nigeria with optimal control, Results Phys. 20 (2021) 104598.

[18] A. Zeb, E. Alzahrani, V.S. Erturk, G. Zaman, Mathematical model for coronavirus disease 2019 COVID-19 containing isolation class, Biomed. Res. J. (2020) 3452402.

[19] F. Bai, F. Brauer, The effect of face mask use on COVID-19 models, Epidemiologia 2 (2021) 75–83.

[20] A. Trivedi, N.K.S.D. Makinde, S. Rao, Modeling the spread and control of COVID-19, Systems 9 (2021) 53.

[21] R.I. Gweryina, C.E. Madubueze, F.S. Kaduna, Mathematical assessment of the role of denial on COVID-19 transmission with non-linear incidence and treatment functions, Sci. Afr. 12 (2021) e00811.

[22] T. Rume, S.M.D. Islam, Environmental effects of COVID-19 pandemic and potential strategies of sustainability, Heliyon 6 (2020) e04965.

[23] P.A. Naik, J. Zu, M.B. Ghori, M. Naik, Modeling the effects of the contaminated environments on COVID-19 transmission in India, Results Phys. 29 (2021) 104774.

[24] A.K. Paul, M.A. Kuddus, Mathematical analysis of a COVID-19 model with double dose vaccination in Bangladesh, Results Phys. 35 (2022) 105392.

[25] M.L. Diagne, H. Rwezaura, S.Y. Tchoumi, J.M. Tchuenche, A mathematical model of COVID-19 model with vaccination and treatment, Comput. Math. Methods Med. (2021) 1250129.

[26] N. Kojima, J.D. Klausner, Protective immunity after recovery from SARS-CoV-2 infection, Lancet Infect. Dis. 22 (1) (2022) 12–14.

[27] K. Sharun, K. Dhama, A.M. Pawde, et al., SARS-CoV-2 in animals; potential for unknown reservoir hosts and public health implications, Vet. Q. 41 (1) (2021) 181–201.

[28] H.S. Rahman, M.S. Aziz, R.H. Hussein, et al., The transmission modes and sources of COVID-19: a systematic review, Int. J. Surg. Open 26 (2020) 125–136.

[29] P.V. den Driessche, J. Watmough, Reproduction numbers and sub-threshold endemic equilibria for compartmental models of disease transmission, J. Math. Biosci. 180 (2002) 29–48.

[30] J.M. Heffernan, R.J. Smith, L.M. Wahl, Perspectives on the basic reproduction ratio, J. R. Soc. Interface 2 (2005) 281–293.

[31] K.H. Hntsa, B.N. Kahsay, Analysis of cholera epidemic controlling using mathematical modelling, Int. J. Math. Math. Sci. (2020) 7369204.

[32] J.P.L. Salle, The Stability of Dynamical Systems, Hamilton Press, Berlin, New Jersey, USA, 1976.

[33] A.B. Gumel, C.C. McCluskey, J. Watmough, An SVEIR model for assessing potential impact of an imperfect anti-SARS vaccine, Math. Biosci. Eng. 3 (3) (2006) 485–512.

[34] M.S. Goudiaby, L.D. Gning, M.L. Diagne, B.N. Dia, H. Rwezaura, J.M. Tchuenche, Optimal control analysis of a COVID-19 and tuberculosis co-dynamics model, Inf. Med. Unlocked (2022).

[35] C. Castillo-Chavez, B. Song, Dynamical models of tuberculosis and their applications, Math. Biosci. Eng. 1 (2) (2004) 361–404.

[36] M. Martcheva, An Introduction to Mathematical Epidemiology, vol. 61, Springer Science and Business Media, 2015.

[37] Centers for Disease Control and Prevention (CDC), Clinical guidance for Covid-19 vaccination. Retrieved on July 8, 2022 from https://www.cdc.gov/vaccines/covid-19/clinical-considerations/interim-considerations-us.html~(2022).

[38] G.T. Tilahun, O.D. Makinde, D. Malonza, Modelling and optimal control of pneumonia disease with cost-effectiveness strategies, J. Biol. Dyn. 11 (52) (2017) 400–426.

[39] J.K.K. Asamoah, E. Okyere, A. Abidemi, S.E. Moore, et al., Optimal control and comprehensive cost-effectiveness analysis for COVID-19, Results Phys. 33 (2022) 105177.

[40] D. Ghafoor, Z. Khan, D. Ualiyeva, N. Zaman, Excessive use of disinfectants against COVID-19 posing a potential threat to living beings, Curr. Res. Toxicol. 2 (2021) 159–168.

[41] K. Dhama, S.K. Patel, R. Kumar, R. Masand, J. Rana, et al., The role of disinfectants and sanitizers during COVID-19 pandemic: advanges and deleterious effects on humans and environment, Environ. Sci. Pollut. Res. 28 (2021) 34211–34228.